ECSS-E-HB-31-01 Part 16A
5 December 2011

Space engineering

Thermal design handbook - Part 16: Thermal Protection System

ECSS Secretariat
ESA-ESTEC
Requirements & Standards Division
Noordwijk, The Netherlands

Foreword

This Handbook is one document of the series of ECSS Documents intended to be used as supporting material for ECSS Standards in space projects and applications. ECSS is a cooperative effort of the European Space Agency, national space agencies and European industry associations for the purpose of developing and maintaining common standards.

The material in this Handbook is a collection of data gathered from many projects and technical journals which provides the reader with description and recommendation on subjects to be considered when performing the work of Thermal design.

The material for the subjects has been collated from research spanning many years, therefore a subject may have been revisited or updated by science and industry.

The material is provided as good background on the subjects of thermal design, the reader is recommended to research whether a subject has been updated further, since the publication of the material contained herein.

This handbook has been prepared by ESA TEC-MT/QR division, reviewed by the ECSS Executive Secretariat and approved by the ECSS Technical Authority.

Disclaimer

Published by: ESA Requirements and Standards Division
ESTEC, P.O. Box 299,
2200 AG Noordwijk
The Netherlands

Table of contents

Figures

1
Scope

The thermal protection system (TPS) of a space vehicle ensures the structural integrity of the surface of the craft and maintains the correct internal temperatures (for crew, electronic equipment, etc.) when the vehicle is under the severe thermal loads of re-entry. These loads are characterised by very large heat fluxes over the relatively short period of re-entry.

The design of thermal protection systems for re-entry vehicles is very complex due to the number and complexity of phenomena involved: the flow around the vehicle is hypersonic, tridimensional and reactive, and its interaction with the vehicle's surface may induce chemical reactions which are not fully understood.

Two TPS concepts for re-entry vehicles, ablative and radiative are examined and there is also an anlyisis of existing systems using them.

The Thermal design handbook is published in 16 Parts

ECSS-E-HB-31-01 Part 1A	Thermal design handbook – Part 1: View factors
ECSS-E-HB-31-01 Part 2A	Thermal design handbook – Part 2: Holes, Grooves and Cavities
ECSS-E-HB-31-01 Part 3A	Thermal design handbook – Part 3: Spacecraft Surface Temperature
ECSS-E-HB-31-01 Part 4A	Thermal design handbook – Part 4: Conductive Heat Transfer
ECSS-E-HB-31-01 Part 5A	Thermal design handbook – Part 5: Structural Materials: Metallic and Composite
ECSS-E-HB-31-01 Part 6A	Thermal design handbook – Part 6: Thermal Control Surfaces
ECSS-E-HB-31-01 Part 7A	Thermal design handbook – Part 7: Insulations
ECSS-E-HB-31-01 Part 8A	Thermal design handbook – Part 8: Heat Pipes
ECSS-E-HB-31-01 Part 9A	Thermal design handbook – Part 9: Radiators
ECSS-E-HB-31-01 Part 10A	Thermal design handbook – Part 10: Phase – Change Capacitors
ECSS-E-HB-31-01 Part 11A	Thermal design handbook – Part 11: Electrical Heating
ECSS-E-HB-31-01 Part 12A	Thermal design handbook – Part 12: Louvers
ECSS-E-HB-31-01 Part 13A	Thermal design handbook – Part 13: Fluid Loops
ECSS-E-HB-31-01 Part 14A	Thermal design handbook – Part 14: Cryogenic Cooling
ECSS-E-HB-31-01 Part 15A	Thermal design handbook – Part 15: Existing Satellites
ECSS-E-HB-31-01 Part 16A	Thermal design handbook – Part 16: Thermal Protection System

2
References

ECSS-S-ST-00-01 ECSS System - Glossary of terms

All other references made to publications in this Part are listed, alphabetically, in the **Bibliography**.

3
Terms, definitions and symbols

3.1 Terms and definitions

For the purpose of this Standard, the terms and definitions given in ECSS-S-ST-00-01 apply.

3.2 Abbreviated terms

The following abbreviated terms are defined and used within this Standard.

CAD	computer aided design
CFD	computational fluid dynamics
CMC	ceramics matrix composite
C/SiC	carbon reinforced silicon carbide
FEI	flexible external insulation
FRSI	flexible reusable surface insulation
HTI	high temperature insulation
HRSI	high-temperature reusable surface insulation
IFI	internal flexible insulation
LRSI	low-temperature reusable surface insulation
RCC	reinforced carbon-carbon
RSI	reusable surface insulation
SIP	strain isolation pad
SOML	structural outer mold line
TOML	TPS outer mold line
TPS	thermal protection system

4 Introduction

4.1 General

The thermal protection system (TPS) of a space vehicle consists of those elements needed to protect the structural integrity of the vehicle's surface and maintain the appropriate internal temperatures (for crew, electronic equipment, etc.) when the vehicle is under the severe thermal loads of re-entry. These loads are mainly characterised by very large heat fluxes during relatively short times.

The heat fluxes acting on the TPS are so large because of the great speeds of re-entry vehicles. The velocity-altitude map for the Space Shuttle is represented in Figure 4-1.

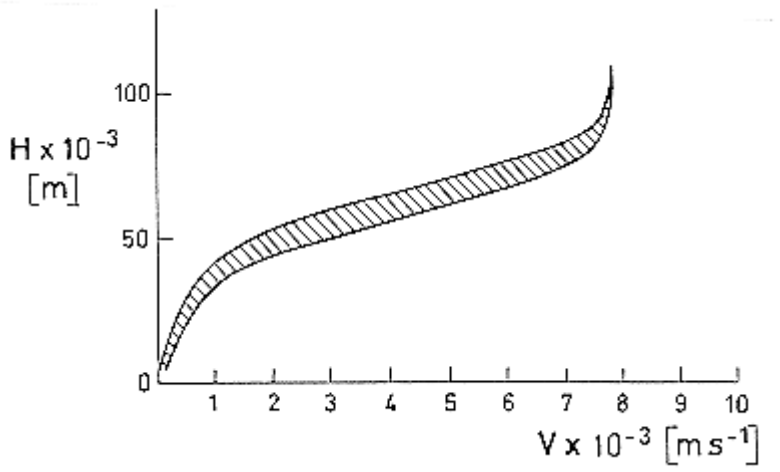

Figure 4-1: Velocity-altitude map for the Space Shuttle. Lifting re-entry from orbit.

The heat fluxes and the time of re-entry are basically determined by the re-entry orbit. These orbits are designed so that the vehicle is captured by the planet and the payload is not damaged by the accelerations; these factors greatly restrict the number of valid trajectories. However, for lifting vehicles which can be manoeuvred those restrictions are alleviated, and re-entry trajectories, other than ballistic, can be achieved. In Figure 4-2 the heat fluxes and re-entry times for different trajectories are summarised.

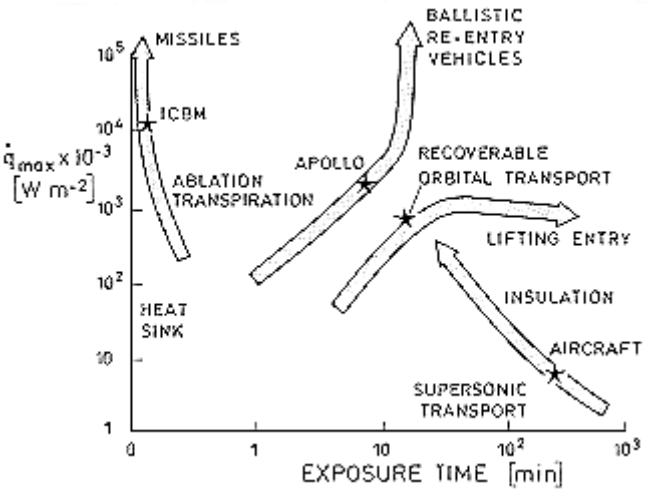

Figure 4-2: Summary of re-entry trajectories. From East (1991) [6].

The design of thermal protection systems for re-entry vehicles is a very complex problem due to the number and complexity of phenomena involved. It suffices to mention here that the flow around the vehicle is hypersonic, tridimensional and reactive, and its interaction with the vehicle's surface may induce chemical reactions which are not fully understood.

4.2 Classification of thermal protection systems

Generally speaking the TPS consists of a material system (shield and/or load carrying member) operating on a given heat dissipation principle. There are several TPS concepts for re-entry vehicles (Hurwicz & Rogan (1973a) [9]):

- Ablative thermal protection
- Radiative thermal protection
- Heat sinks
- Transpiration cooling

ABLATIVE SYSTEMS

Ablative systems operate dissipating the incident thermal energy through the loss of material: these systems lose mass as a consequence of the ablation of the external surface material. They have good thermal characteristics since phase changes absorb a large amount of energy. These systems are not reusable. See Figure 4-3 for a sketch of an ablative system.

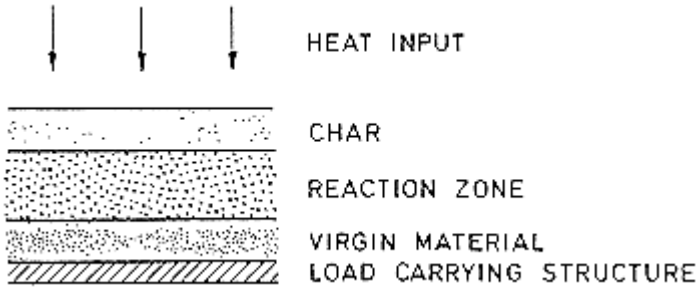

Figure 4-3: Sketch of an ablative thermal protection system.

The ablation process is quite complex and is described in some detail in clause 5.2. One important consequence of the analysis of these systems is that their efficiency is particularlysensitive to material performance. Therefore, it is necessary to treat the subject of materials in detail. In the absence of a universally acceptable ablative material a wide variety of ablative compositions and constructions have been produced, usually tailored to satisfy the requirements of a specific vehicle for a specific mission. A detailed description of ablative materials is given in clause 5.3.

RADIATIVE SYSTEMS

Radiative systems operate re-emitting by radiation the energy received from the surrounding environment. They are composed of two layers: an outer layer which consists of a material that can stand the radiation equilibrium temperature and an inner layer which insulates the outer layer from the structure in order to minimise the heat flow between the two, see Figure 4-4.

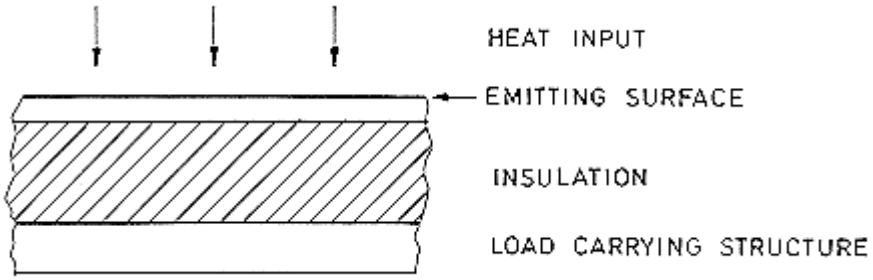

Figure 4-4: Sketch of a radiative thermal protection system.

It will be seen in clause 6.1 that the effectiveness of a radiative system increases very rapidly with increasing surface temperatureand surface emissivity. Consequently, the primary development efforts have been concerned with the improvement of high emissivity, high temperature coatings, and with increasing the material service temperatures (including that of the internal insulation). A detailed description of materials used in radiative systems is given in clause 6.2.

These systems can be designed including a cooling subsystem: this is a fluid loop where the working fluid transports heat from the areas where the heat flux is stronger to those where the heat flux is weaker. The actual mechanism for heat transport can be the same as in heat pipes, the fluid is vaporised in areas of higher temperatures, and it is condensed in areas of lower temperatures. However, even though the characteristics of these systems are good, they are not used in practice.

HEAT SINK THERMAL PROTECTION SYSTEM

A heat sink is the simplest type of absorptive thermal protection system. It was used in the design of the early re-entry vehicles (e.g. the first two manned Mercury vehicles).

These systems are composed of an outer layer, comparatively thick, which consists of a material of high conductivity and capacitance. The function of this layer is to absorb the heat input. Since the material heats up, the storage capability is limited by the melting temperature.

Its use is limited to relatively low heating rates and therefore may not be practical for the high heat loads encountered in short re-entry times.

Heat sinks have the advantages of simplicity, dependability, and for reusable vehicles, ease of refurbishment. Their outstanding disadvantage is their low efficiency, this would cause a heat sink sized to satisfy most current re-entry missions to be excessively heavy.

Materials commonly used as heat sinks are

- beryllium
- beryllium oxide (beryllia)
- copper.

Graphite has many desirable heat sink characteristics, but begins to oxidise at temperatures far below those required for best efficiency.

TRANSPIRATION COOLING

Transpiration systems are systems where fluid is injected through a porous medium into the boundary layer. The structure is maintained cool by two basic mechanisms: heat is conducted to the coolant as it flows through the structure, and as the coolant is ejected out the surface it reduces the surface heat transfer rate by cooling and thickening the boundary layer. See Figure 4-5 for a sketch.

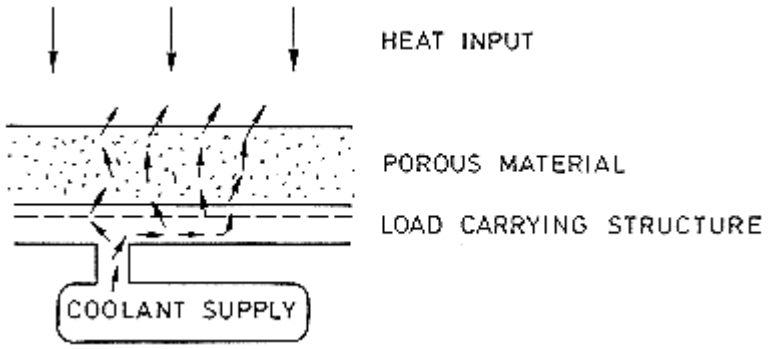

Figure 4-5: Sketch of a transpiration thermal protection system.

In some applications, the shape change caused by the surface recession of an ablating surface is not acceptable for aerodynamic performance reasons. In such cases, if the environment is too severe for radiative or heat sink systems, transpiration cooling may be the only practical solution. This TPS makes possible performance in environments that could not otherwise be withstood. However, its mechanical complexity (see Figure 4-6), with the associated reliability problems, tend to limit its use.

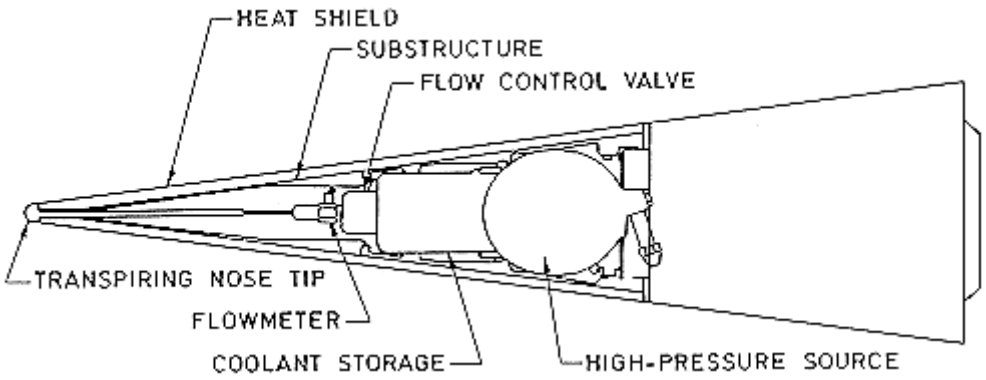

Figure 4-6: Typical transpiration cooling system

For re-entry application, the most acceptable coolants are:

- H_2O
- NH_3
- CF_4
- CO_2

5
Ablative systems

5.1 General

The ablation mechanism for thermal protection is based on the sublimation, melting or pyrolysis of the heat shield and the removal of the products by the outer stream. The great amount of energy absorbed in phase transition reduces the heat fluxes to the structure of the vehicle. This method has been widely used in most of non–reusable entry vehicles, for its simplicity and its high performance. It has been used in planetary probes, ballistic missiles and space capsules.

The methods of analysing the various heat shield materials vary depending on the melt temperature and oxidation chemistry. These materials may be classified as

a. Oxidation controlled. The melting temperature is greater than the radiative equilibrium temperature calculated for the convective heat transfer rate.

b. Simple sublimers. When melting temperature is lower than the radiative equilibrium temperature.

c. Pyrolytic ablators. The material decomposition into pyrolysis gas and char occurs in depth.

Despite the above classification almost all heat shields are made with carbon based materials. This fact is due to special characteristic combination of very desirable properties as good heat sink, high melt temperature, large heat of sublimation, good radiation properties, and from the structural point of view low dilatation coefficient.

5.2 Ablative materials

Materials commonly used can be classified as follows:

Composites:

Carbon phenolic:

High strength charring ablator with high ablation temperature.

Used in high performance re-entry vehicles.

It is the current heat shield material choice.

Used in the Galileo probe (clause 5.4.1).

Silica phenolic:

High strength charring ablator.

Used in high performance re-entry vehicles.

Selected for the Huygens probe.

Phenolic nylon:

High heat shielding capability.

It has the disadvantage of high erosion rate.

Limited capability to accommodate high heat loads.

Used in the Galileo probe aft shield (clause 5.4.1).

Ceramics:

Graphite:

Used in high heating rate areas.

It has disadvantages as brittleness and low resistance to thermal stress.

ATJ graphite has high strength properties.

Metals:

Tungsten:

Refractory metal.

Used as a porous matrix infiltrated with copper or silver.

It has good mechanical properties but low thermal performance.

Elastomers:

Silicone polymers:

Used reinforced by ceramic microspheres.

Used in low shear and low pressure regions, and in low to moderate heat flux zones.

It was used in the Gemini project.

Plastics:

Teflon:

Low temperature ablator with moderate efficiency and high ablation rates.

It has been used in ballistic missiles.

AVCOAT 5026.

Ablator used in the Apollo capsules.

5.3 Basic analysis

The methods for predicting surface degradation or recession of ablative thermal protection systems have been purely empirical or semitheoretical. The semitheoretical methods are based on simplifying assumptions that will be explained later. These simplifications are due to the extremely complicated physico-chemical phenomena involved in the ablation process. It includes phase change, non–equilibrium effects, multiphase flow, high thermal radiation environment, three dimensional hypersonic flow. The design of high mass heat shields has made it necessary accurate theoretical

models for ablation. An accurate design of these heat shields is critical due to the high mass of ablator necessary for protecting the vehicles. It can be noticed that heavy heat shields may make missions not feasible. An example of accurate theoretical design is the Galileo Jovian probe, it has been designed using numerical detailed flow field predictions, despite the uncertainties on the Jupiter atmosphere composition.

5.3.1 Surface equilibrium

To establish the energy flux to the re-entry vehicle, the energy transfer mechanisms between the boundary layer and the ablating surface of the vehicle must be stated. Despite the fact that the ablation problem is non–steady, the assumption of steady state will be made. This approximation is rather accurate for engineering purposes. It is assumed, also, that the fluid flow near the surface is governed by the equations of the boundary layer with mass injection. In this analysis (Hurwicz & Rogan (1973b) [10]) the conservation of mass and energy are applied to a thin control volume (since this is a moving control volume the Reynolds transport theorem should be taken into account).

First the mass balance is considered. The mass flux leaving the control volume through the gas side is due to gaseous species, that are denoted by $\dot{m}_w$, plus solid and liquid species, denoted by $\dot{m}_r$ .The term $\dot{m}_w$ is due to sublimation of the heat shield and products from pyrolysis reactions that occur in the heat shield. The term $\dot{m}_r$ is due to mechanical erosion of liquid and solid products, the solid erosion is due to spallation of solid particles and to the surface stress due to percolation and sublimation, the liquid products are due to heat shield melting. This term, $\dot{m}_r$, should be reduced because this mass does not sublime, thus reducing the performance of the heat shield. The mass flux entering the control volume through the solid side is due to the products of pyrolysis reactions that occur in the heat shield, and to the solid mass that enters due to the movement of the control volume. The first flux is denoted by $\dot{m}_{g_s}$ and the second one by $\dot{m}_{c_s}$. The continuity equation yields

$$\dot{m}_w + \dot{m}_r = \dot{m}_{c_s} + \dot{m}_{g_s} \qquad [5\text{-}1]$$

with

$$\dot{m}_{c_s} = \sum_{k'} \left(\dot{m}_{k'}\right)_w \quad , \quad \dot{m}_{g_s} = \sum_{k''} \left(\dot{m}_{k''}\right)_w \qquad [5\text{-}2]$$

where *k′* denotes summation over all the solid species entering the control volume, and *k*'' denotes summation over the gaseous species.

The energy balance yields

$$\begin{aligned} \dot{q}_s = \dot{q}_w - \dot{m}_w h_w - \dot{m}_r h_r + \dot{m}_{c_s} h_{c_s} + \\ + \dot{m}_{g_s} h_{g_s} - \varepsilon_w \sigma T_w^4 + \alpha_w \dot{q}_{rad} \end{aligned} \qquad [5\text{-}3]$$

where the meaning of each term is explained below.

$\dot{q}_s$ is the energy flux to the solid, it is positive when the energy flux is to the solid.

$\dot{q}_w$ is the energy flux due to the aerodynamic heat transfer to the ablator from the boundary layer.

$\dot{m}_w h_w$ is the energy flux associated to the gaseous mass coming into the boundary layer from the solid boundary.

$$h_w = \sum_i Y_i (h_i)_w \qquad [5\text{-}4]$$

with

$$(h_i)_w = \int_{T_o}^{T_w} c_{p_i} dT + h_i^o \qquad [5\text{-}5]$$

where Y_i is the mass fraction of the i-th gaseous species and h_i^o is the formation enthalpy at a reference state (p_o,T_o).

$\dot{m}_r h_r$ is the energy flux associated to the solid and liquid removal from the solid boundary.

$\dot{m}_{c_s} h_{c_s}$ is the energy flux corresponding to the solid mass flux associated to the recession of the heat shield.

$$\dot{m}_{c_s} h_{c_s} = \sum_{k'} (\dot{m}_{k'})_w (h_{k'})_w \qquad [5\text{-}6]$$

$\dot{m}_{g_s} h_{g_s}$ is the energy flux corresponding to the gas mass flux associated to pyrolisis reactions.

$$\dot{m}_{g_s} h_{g_s} = \sum_{k''} (\dot{m}_{k''})_w (h_{k''})_w \qquad [5\text{-}7]$$

$\varepsilon_w \sigma T_w^4$ is the energy flux radiated by the solid surface, where ε_w is the surface emissivity and σ is the Stefan-Boltzman constant.

$\alpha_w \dot{q}_{rad}$ is the energy flux absorbed from the fluid, where α_w is the absorptance; $\dot{q}_{rad}$ should be obtained from the shock layer solution.

In Figure 5-1 the surface energy balance is sketched, where the different quantities appearing in the equation are positive if the fluxes have the sense shown in the figure.

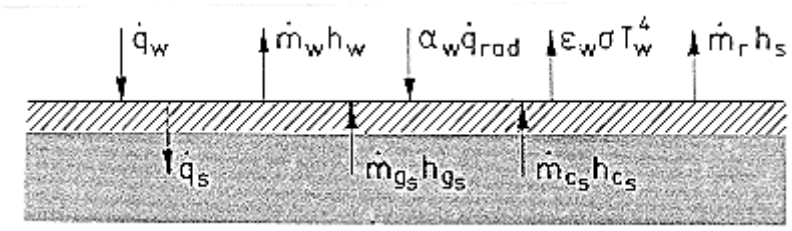

Figure 5-1: Surface energy balance

In order to make use of the previous analysis, the different terms in the energy balance need to be evaluated. This is a difficult interdisciplinary task. As an example some results for the aerodynamic heating from the boundary layer, $\dot{q}_w$, are summarised here.

For air, Fay and Riddle (quoted in Anderson (1989) [1]) have correlated many experimental results obtaining different correlations for the heat flux at the stagnation point of a spherical nose. For equilibrium boundary layer the heat flux is

$$\dot{q}_w = 0{,}76 Pr^{-0{,}6} \left(\rho_e \mu_e\right)^{0{,}4} \left(\rho_w \mu_w\right)^{0{,}1} \sqrt{\frac{du_e}{ds}} \left(l_e - h_w\right) \left[1 + \left(Le^{0{,}52} - 1\right) \frac{h_c}{l_e}\right] \quad [5\text{-}8]$$

For a frozen boundary layer with a fully catalytic wall

$$\dot{q}_w = 0{,}76 Pr^{-0{,}6} \left(\rho_e \mu_e\right)^{0{,}4} \left(\rho_w \mu_w\right)^{0{,}1} \sqrt{\frac{du_e}{ds}} \left(l_e - h_w\right) \left[1 + \left(Le^{0{,}63} - 1\right) \frac{h_c}{l_e}\right] \quad [5\text{-}9]$$

For a frozen boundary layer with a noncatalytic wall

$$\dot{q}_w = 0{,}76 Pr^{-0{,}6} \left(\rho_e \mu_e\right)^{0{,}4} \left(\rho_w \mu_w\right)^{0{,}1} \sqrt{\frac{du_e}{ds}} \left[1 - \frac{h_c}{l_e}\right] \quad [5\text{-}10]$$

where

$$Pr = \frac{\mu_e c_{p_e}}{k_e} \text{ Prandtl> number} \quad [5\text{-}11]$$

$$Le = \frac{\rho_e c_{p_e} D}{k_e} \text{ Lewis> number} \quad [5\text{-}12]$$

ρ_e density outside the boundary layer

μ_e viscosity outside the boundary layer

k_e thermal conductivity outside the boundary layer

c_{pe} specific heat at constant pressure outside the boundary layer

D diffusion coefficient

ρ_w density at the wall

μ_w viscosity at the wall

I_e total enthalpy of the stream outside the boundary layer

$$I_e = \int_{T_o}^{T_e} c_p dT + \frac{U_e^2}{2} \qquad [5\text{-}13]$$

where U_e is the velocity outside the boundary layer

h_w enthalpy at the wall

$$h_w = \int_{T_o}^{T_e} c_p dT \qquad [5\text{-}14]$$

$$h_c = \sum_i (Y_i)_e h_i^o \qquad [5\text{-}15]$$

where $(Y_i)_e$ is the mass fraction of the i-th species outside the boundary layer and h_i^o is the formation enthalpy of the i-th species at the reference state

and the stagnation point velocity gradient is given by Newtonian theory (Anderson (1989) [1]) as

$$\frac{du_e}{ds} = \frac{1}{R}\sqrt{\frac{2(p_e - p_\infty)}{\rho_e}} \qquad [5\text{-}16]$$

where p_e is the pressure outside the boundary layer, $p\infty$ the pressure far ahead of the spherical nose, and R is the local radius of curvature of the body at the stagnation point.

5.4 Existing systems

5.4.1 Galileo probe

The mission of the Galileo entry probe is to descend through Jupiter's atmosphere, and it is instrumented so that the planet's atmospheric structure, composition, and radiation balance can be measured. The probe is illustrated in Figure 5-2. The main components are the descent module, which contains the scientific measurement package, the aeroshell structure and the thermal protection system. The TPS consists of two heat shields, one for the forebody and another for the afterbody. The forebody shield consists of two parts, the spherical nose composed of chopped-molded carbon phenolic, and the frustrum composed of 30° tape-wrapped carbon phenolic. The probe aft shield is made of phenolic nylon. The ablative material is bonded to the aeroshell which is made of aluminium.

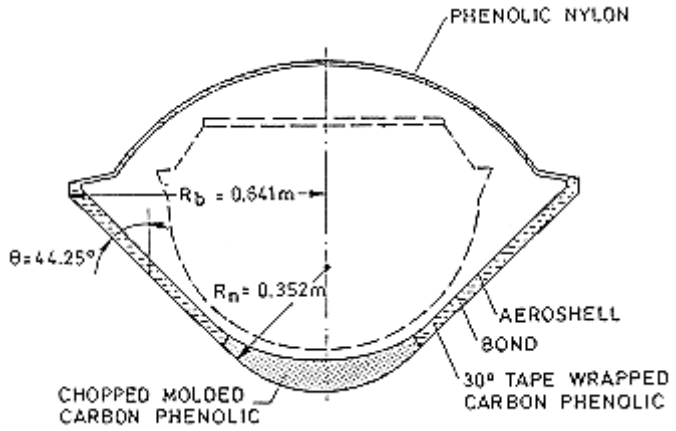

Figure 5-2: Galileo entry probe.

In this clause the study on the ablative thermal protection system made by Green and Davy (1982) [8] will be described. This study corresponds to a 310 kg probe (other studies for a 242 kg and a 290 kg probes are also available). The actual probe mass is 339 kg.

5.4.1.1 Heat shield analysis

The analysis of the heat-shield is divided into four parts which are described next (see Figure 5-3).

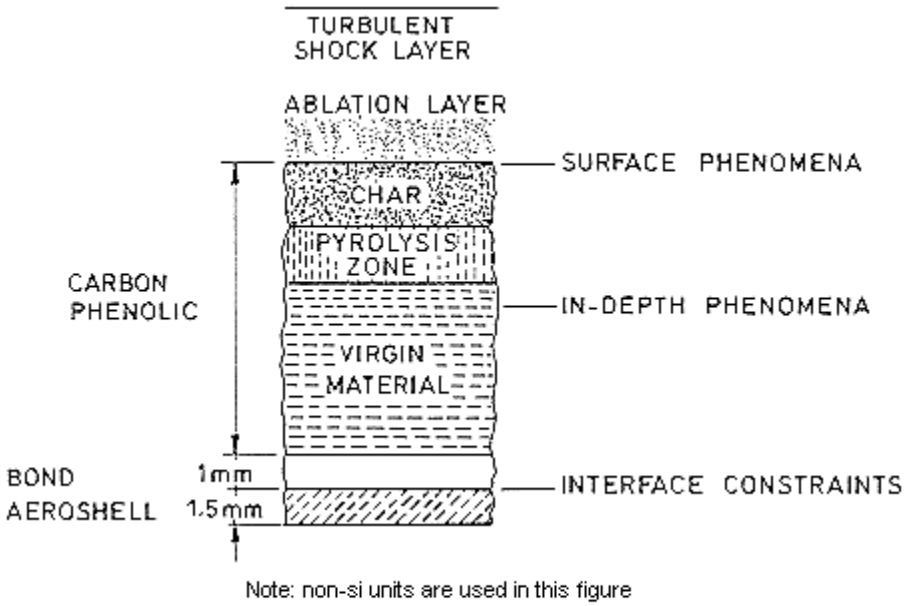

Figure 5-3: Physical model and phenomena considered in material response analysis

1. Specifying the entry heating environment.
2. Modelling the in-depth phenomena:
    - conduction
    - receding surface
    - decomposition
    - pyrolysis
    - storage
3. Modelling the surface phenomena:
    - ablative heating
    - reradiation
    - equilibrium chemistry
    - ablation
    - elemental mass diffusion
    - char removal
    - pyrolysis
4. Specifying the interface constraints necessary to size the shield. In this case they are the following:
    - bond temperature less than 644 K
    - aeroshell temperature less than 589 K
    - insulated back surface of the aeroshell

This analysis also requires knowledge of material properties for the carbon-phenolic (including the char), the bond and the aeroshell.

5.4.1.2 Results

The different models (including material-property models) used in the analysis are described in Green and Davy (1982) [8]. In this clause some results will be presented. In Figure 5-4 the response at the three key interfaces is shown; results for two models, quasi-steady and transient, are presented. The difference in maximum temperature between both models is about 5%. The mass loss fluxes are presented in Figure 5-5. The time-integrated mass loss indicates that the quasi-steady result is about 20% higher. It can be noted that these differences are actually due to the use of different material-property models.

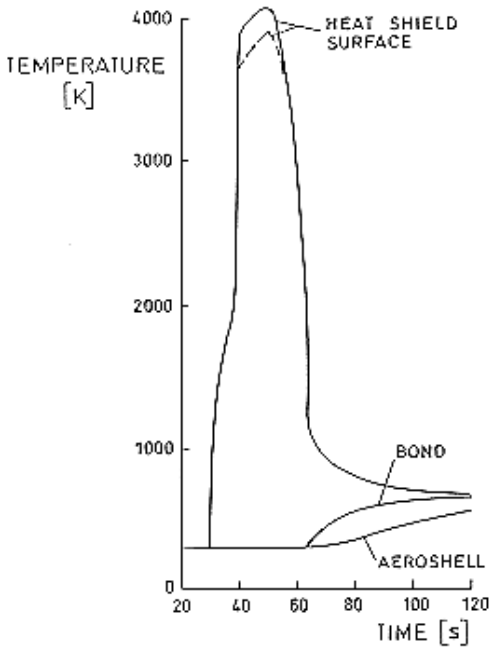

Figure 5-4: Temperature history at interfaces.

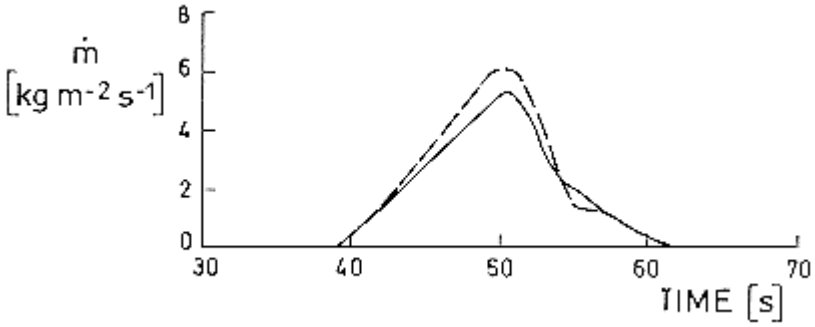

Figure 5-5: Comparison of mass loss fluxes.

With respect to the total mass of ablator, different material-property models give different results, ranging from 117 kg (of which 93 kg is lost) to 139 kg (of which 120 kg is lost). The principal difference in these models is the value of the surface reflectance. The heat-shield mass requirement is so large (around 40% of the total mass) that a heat-shield design based on a conservative safety margin, although desirable, is not possible, except at the expense of other subsystems, because the total probe mass is constrained by launch requirement limits. Hence, an accurate heat-shield design is crucial to the success of the mission.

6
Radiative systems

6.1 General

In this second class of thermal protection systems there is no mass loss; these systems can be reused. The thermal protection is achieved by re-emitting in form of thermal radiation the energy received by the solid walls.

In these systems energy absorption is small, and thus the surface energy balance can be expressed as

$$\dot{q}_w = \sigma \varepsilon_w T_w^4 \qquad [6\text{-}1]$$

where T_w is the radiation equilibrium temperature and is the maximum temperature the surface can experience for a given heat flux. The radiative system is therefore limited to a maximum heat rate (by virtue of its operating temperature limit) rather than a total heat input as an ablator may be. Once an operating temperature limit is defined, the maximum heat flux is correspondingly defined and the system can operate indefinitely at this condition. The penalty associated with increased operating time is the amount of insulation required between the heat shield and inner surface (either the load carrying structure or the payload).

As evidenced by the equation above, the effectiveness of a radiative system increases very rapidly with increasing surface temperature. The surface emissivity, ε, also exerts an important, although lesser, effect on the amount of energy which can be accommodated.

6.2 Radiative materials

External insulators commonly used can be divided in two classes: rigid and flexible.

RIGID INSULATORS

Rigid insulators can adopt different shapes: tiles, shingles, shells and boxes. Materials used to make them can be classified as follows:

Composites:

- Carbon carbon
- Reinforced carbon carbon (see clause 6.3.1.1)
- Carbon/Silicon carbide

Ceramics:

- Sinterized alumina/silica fibres
- Sinterized high-purity silica fibres

This type of insulation is used to protect areas exposed to the highest temperatures.

FLEXIBLE INSULATORS

Flexible insulators are blankets of different materials:

- Silica fibre
- Glass fibre
- Alumina/silica fibre
- Alumina/borosilicate fibre
- Nomex fibre
- Alumina fibre plated with rhodium
- Nylon

These materials are processed into fleeces, felts or threads, which then form the blankets.

6.3 Existing systems

6.3.1 Space shuttle

In this clause the thermal protection system of the Space Shuttle Orbiter will be described. This system is designed so that it can be used 100 times or more without major refurbishment. The surface of the Shuttle is subjected to temperatures ranging from 600 K to 1750 K, as shown in Figure 6-1, and the TPS is designed to keep the vehicle structure at the temperatures shown in Figure 6-2.

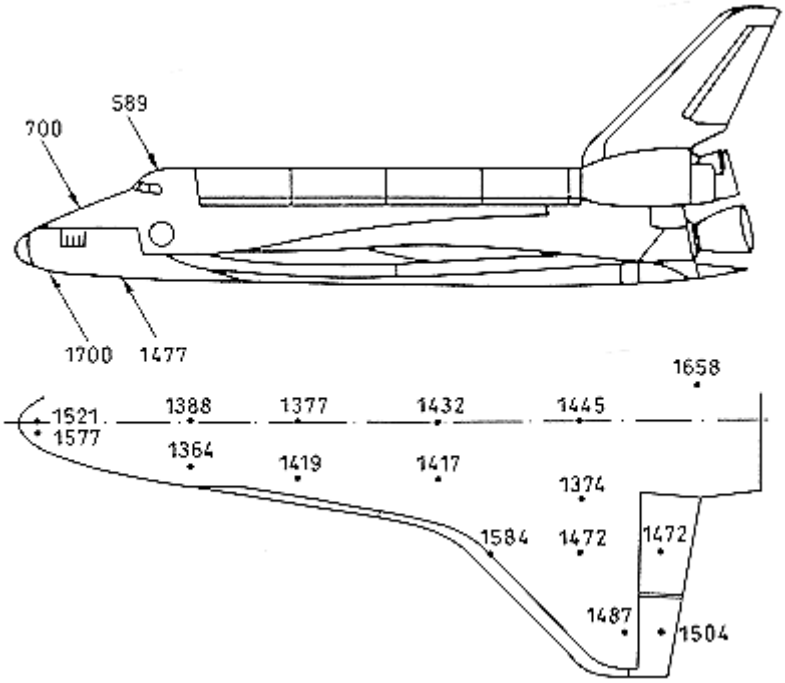

Figure 6-1: Worst case peak predicted surface temperatures. [K] for STS-1. From Dotts et al. (1983) [5].

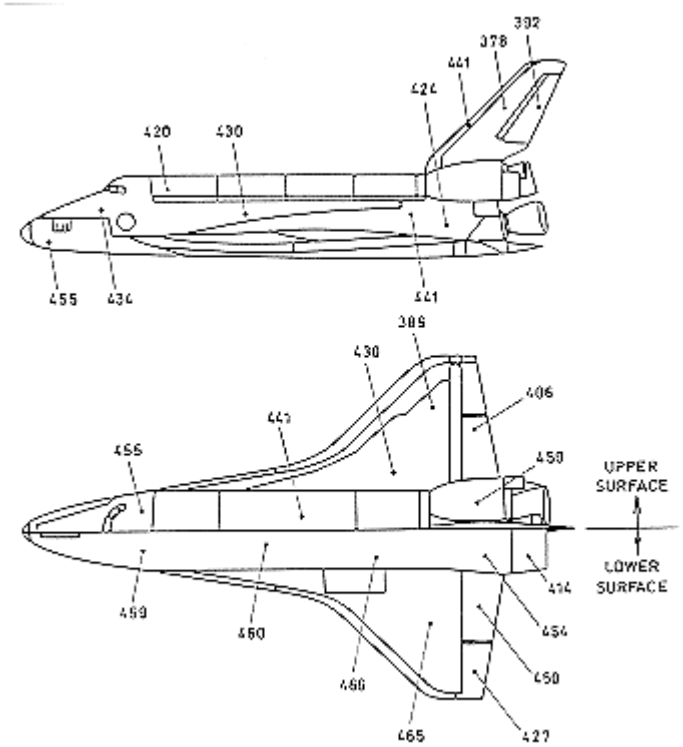

Figure 6-2: Worst case peak predicted structure temperatures. [K] for STS-1. From Dotts et al. (1983) [5].

TPS multimission capability is obtained by a combination of four different material configurations, which are optimised for specific operational temperature ranges.

1. Temperatures greater than 1500 K. The thermal protection subsystem for this region consists of coated reinforced carbon-carbon (RCC).
2. Temperatures from 900 K to 1500 K. This region is protected with a high-temperature reusable surface insulation (HRSI).
3. Temperatures from 650 K to 900 K. In this region the protection is a low-temperature reusable surface insulation (LRSI).
4. Temperatures lower than 650 K. This region is protected with a flexible reusable surface insulation (FRSI).

These four thermal protection subsystems, see Figure 6-3, will be described next.

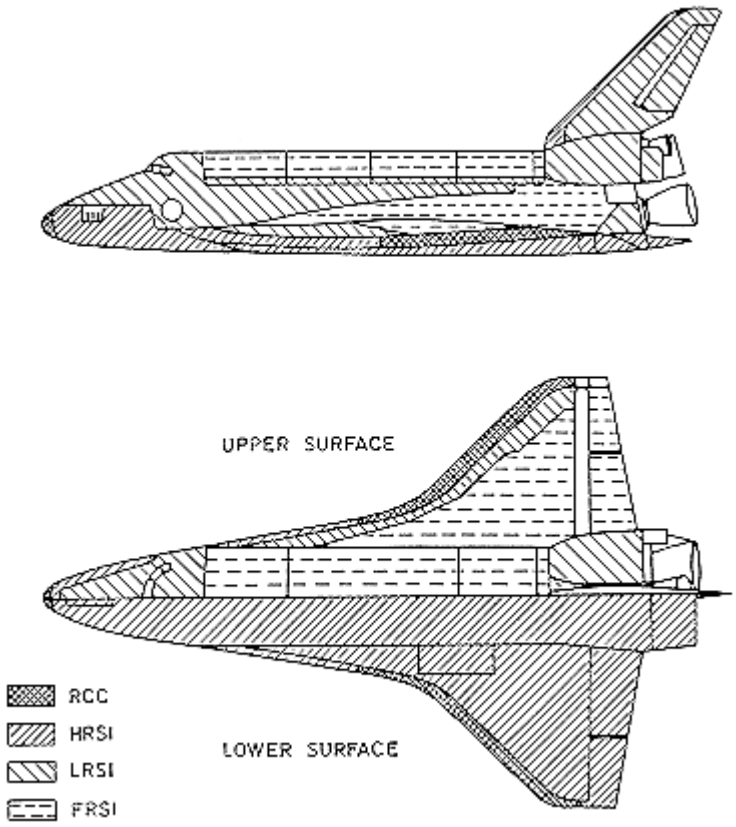

Figure 6-3: Thermal protection subsystems. From Dotts et al. (1983) [5]

6.3.1.1 Description of thermal protection subsystems

REINFORCED CARBON-CARBON

This subsystem consists of the RCC nose cap and RCC wing leading-edge panels, the metallic attachments to the Orbiter structure, the internal insulation system, thermal barriers, and the interface tiles between the RCC and reusable surface insulation (RSI).

The RCC panels function as the airfoil shape at temperatures exceeding 1500 K. The wing leading edge consists of 44 RCC panels/T–seals (22 on each wing), whereas the nose cap is a RCC monoconic shell with associated seals. Figure 6-4, Figure 6-5 and Figure 6-6 show the major components of the nose cap and wing leading-edge systems.

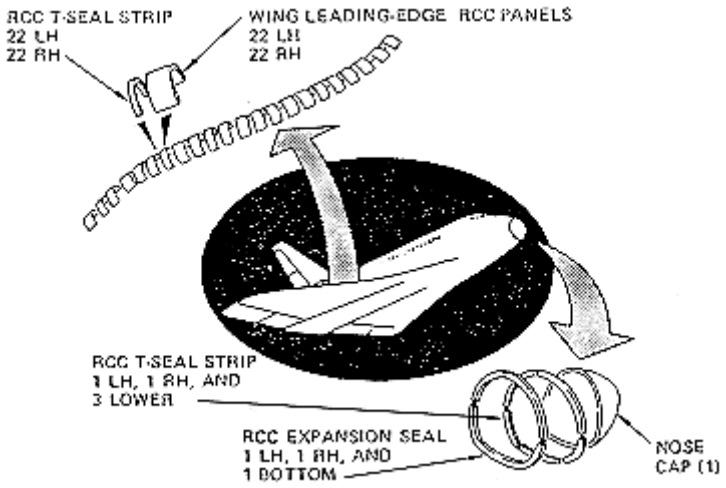

Figure 6-4: RCC system components. From Curry et al. (1983) [3].

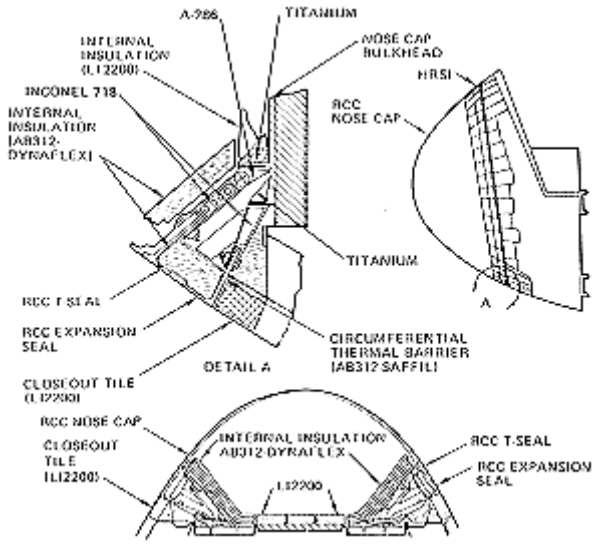

Figure 6-5: Nose cap system components. From Curry et al. (1983) [3].

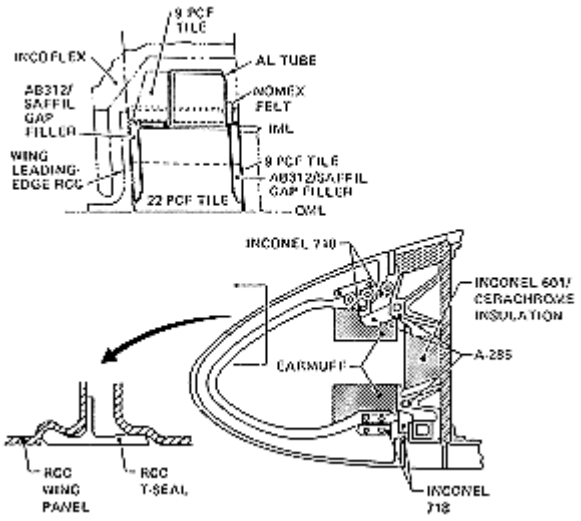

Figure 6-6: Wing leading-edge system components. From Curry et al. (1983) [3].

The RCC material is a hard carbon structure highly resistant to fatigue loads, possessing reasonable strength and a low coefficient of thermal expansion which provides it with excellent resistance to thermal stresses and shock. Since the RCC parts form a hollow shell, they promote internal cross radiation from the hot stagnation region to cooler areas, thus reducing stagnation temperatures and thermal gradients around the shell. The operational temperature of the RCC gets up to about 1900 K.

Since RCC is not an insulator, the adjacent aluminium and the metallic attachments are protected from internal radiant heating by internal insulation. Inconel-covered Dynaflex insulation that is contained in formed and welded Inconel foil protects the metallic attachment fittings from the heat emitted from the inside surface of the RCC wing panels (Figure 6-6). The nose cap internal insulation system (Figure 6-5) consists of blankets fabricated from AB-312 ceramic cloth, saffil and Dynaflex insulation; HRSI tiles protect the forward fuselage from the heat emitted from the hot inside surface of RCC.

RCC attachment

The wing leading edge and nose cap are structural fairings which transmit aerodynamic loads to the forward bulkhead or the wing spar through discrete mechanical attachments. Inconel-718 and A-286 stainless steel fittings are bolted to flanges formed on the RCC components and attached to the aluminium wing spar and fuselage forward bulkhead. The fitting arrangement provides thermal isolation, allows thermal expansion, and accommodates structural displacement. As shown in Figure 6-4, the wing leading edge is a continuous surface consisting of 22 panels joined by 22 T-seals. This segmentation is necessary not only to facilitate the high-temperature fabrication process but is also required to accommodate the thermal expansion during entry of the leading edge while preventing large gaps or interference between the parts. In addition the T-seals prevent the direct flow of hot boundary-layer gases into the wing leading-edge cavity during entry. The nose cap seal design and structural attachment is similar in concept to the wing leading edge described above.

HIGH- AND LOW-TEMPERATURE REUSABLE SURFACE INSULATION

The HRSI and LRSI insulations are fabricated into blocks (ceramic tiles) of high-purity, rigidized silica fibre. The HRSI tiles are nominally 15,24 x 10^{-2} by 15,24 x 10^{-2} m planform and have a thickness in the range 1,27 x 10^{-2} - 10,16 x 10^{-2} m. Approximately 24000 individual HRSI tiles are required to protect the areas of the Orbiter surface exposed to the 900-1500 K temperature range. The LRSI tiles are nominally 20,32 x 10^{-2} by 20,32 x 10^{-2} m planform and have thickness in the range 5 x 10^{-3} - 25,4 x 10^{-3} m. Approximately 6800 individual LRSI tiles are required to protect the areas of the Orbiter surface

exposed to the 650-900 K temperature range. The HRSI tiles have a black borosilicate glass coating on their external surface and four sides. This coating provides a high-emittance surface along with handling and moisture-resistance properties. The LRSI tiles have a white borosilicate glass coating, which also provides a low solar absorptance for orbital thermal control.

The HRSI and LRSI tiles are bonded to the Orbiter surface using a silicone adhesive with an intervening layer of nylon felt material. The tile attachment configuration is shown in Figure 6-7. The nylon felt material strain isolation pad (SIP) prevents thermal and dynamic strains between the ceramic tiles and structure from inducing critical stresses in the ceramic tiles. The SIP is 4 x 10^{-3} m thick. Gaps are provided between the tiles to preclude tile-to-tile contact during the various Orbiter mission environments. For example, the cold extremes of the orbital environment cause the aluminium airframe to contract while the tiles change little because of their low coefficient of thermal expansion. The tile-to-tile gaps are required to accommodate this difference in thermal expansion and preclude tile-to-tile contact damage.

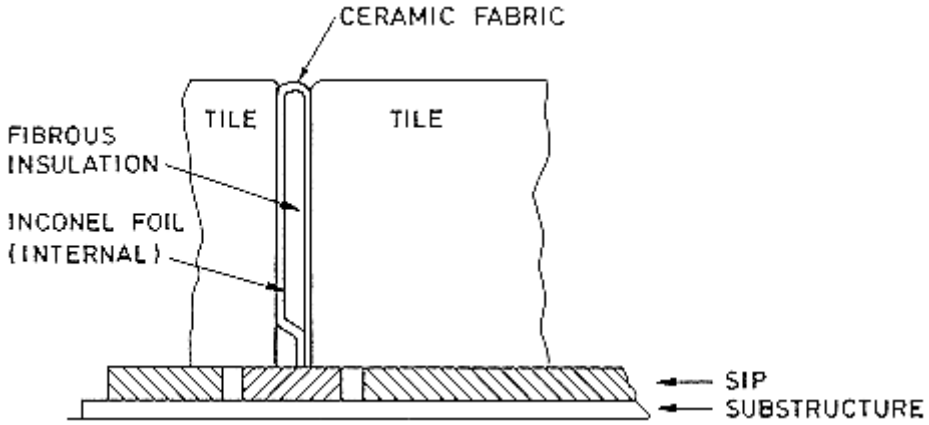

Figure 6-7: Tile attachment and gap filler configuration. From Dotts et al. (1983) [5].

Tile-to-tile gap fillers of woven ceramic cloth are used in regions of high entry-surface-pressure gradient (see Figure 6-7). Without the gap fillers, the high-pressure gradient would cause excessive tile-to-tile gap heating and result in local overtemperature of the tile adhesive bonds, nylon felt, and the Orbiter structure. While gap fillers fill the entire tile-to-tile gap, their flexibility allows for tile movement without damaging the tile sidewalls or resulting in excessive sidewall loads.

Thermal barriers made of woven ceramic cloth wrapped around a high-temperature Inconel wire spring and fibrous insulation are used to fill the tile-to-tile gaps around the Orbiter's movable hatches and doors. Door movement and structural deflections in these regions require large tile-to-tile gaps. These thermal barriers maintain the filled gap requirements throughout the various mission environments.

FLEXIBLE REUSABLE SURFACE INSULATION

The FRSI insulation is a silicone-elastomer-coated nylon felt blanket, bonded to the structure by a silicone adhesive. The FRSI insulation blankets are nominally 0,91 by 1,22 m in planform and are 4 x 10^{-3} - 16 x 10^{-3} m thick. Approximately 315 m^2 of FRSI is required to protect the remaining areas of the Orbiter surface that are exposed to a maximum temperature of 650 K.

6.3.1.2 Thermal response

In this clause the response of the thermal protection subsystems is presented. In particular comparison between thermal mathematical models, test results and flight data is shown.

RCC

Data for the nose cap is presented in Figure 6-8 and Figure 6-9 (peak STS-1/STS-2 RCC shell temperature data were lost, see Figure 6-8). Data for the left wing leading edge (panel 9) is presented in Figure 6-10. The measurements are in excellent agreement with predictions.

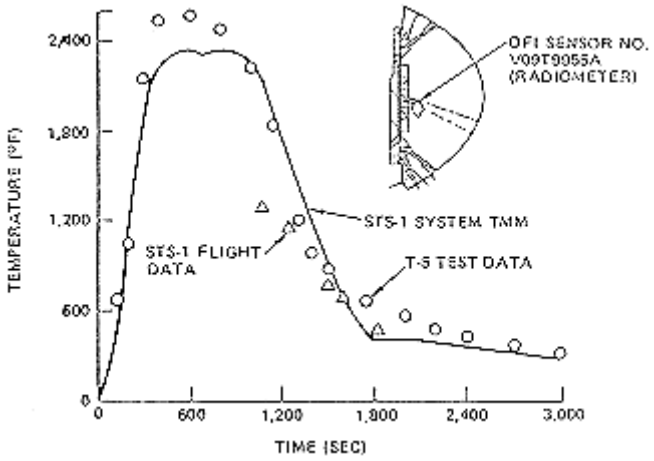

Figure 6-8: Nose cap RCC surface comparison between prediction and flight data. From Curry et al. (1983) [3]

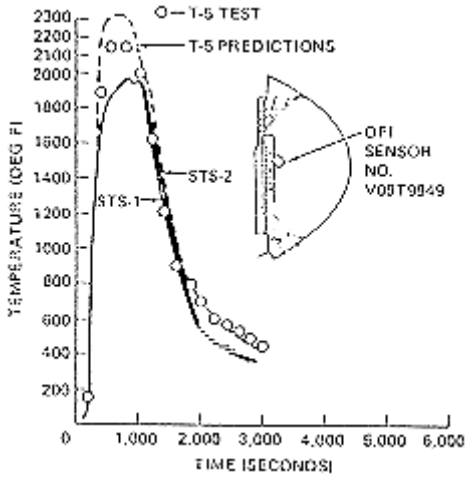

Figure 6-9: Nose cap access door tile surface comparison between prediction and flight data. From Curry et al. (1983) [3].

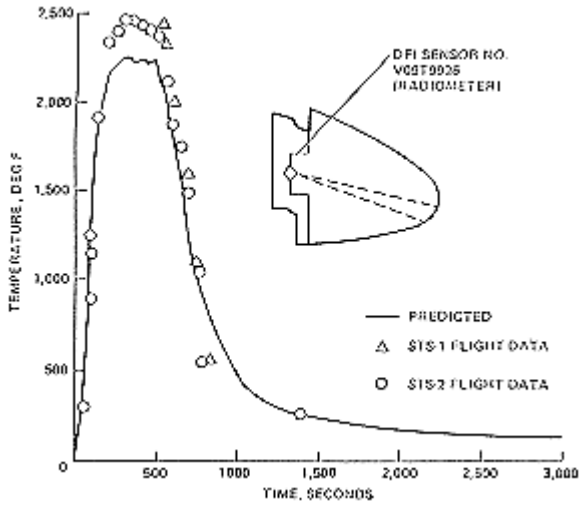

Figure 6-10: Wing leading-edge panel (stagnation area). Comparison between prediction and flight data. From Curry et al. (1983) [3].

HRSI and LRSI

In the following flight data and predicted temperature responses for the RSI are compared. Comparison with flight data for the STS-1 are presented in Figure 6-11 to Figure 6-14, and with data for the STS-2 in Figure 6-15 to Figure 6-17. In the thermal models the RSI measured surface temperature is used as the environmental input. In general, the in-depth RSI, SIP, and structure temperature predictions compare well with the flight responses.

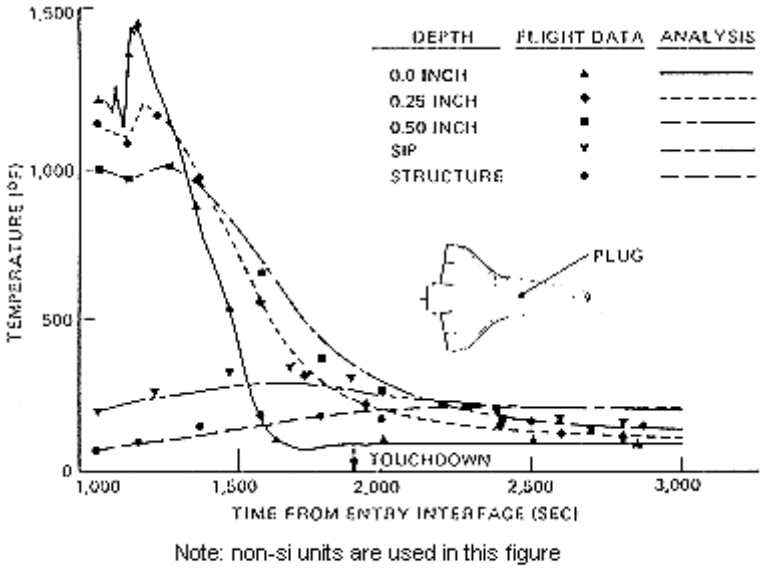

Figure 6-11: STS-1 flight data analysis comparison for lower mid-fuselage location. From Dotts et al. (1983) [3].

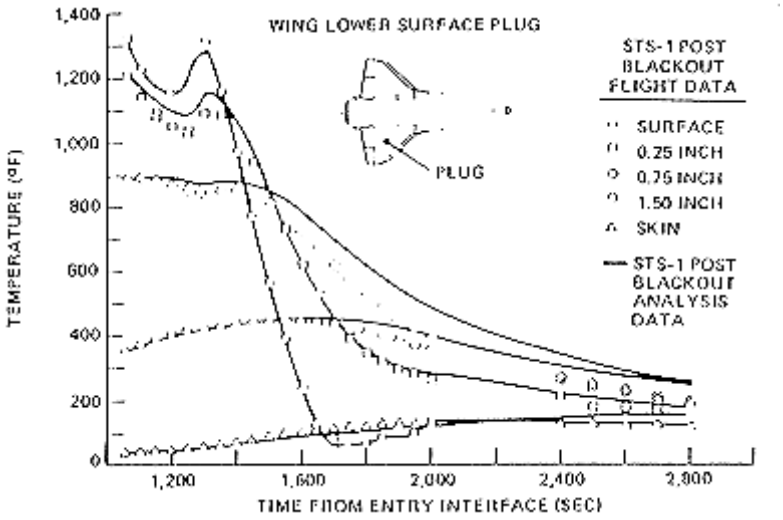

Note: non-si units are used in this figure

Figure 6-12: STS-1 flight data analysis comparison for lower wing location. From Dotts et al. (1983) [3]

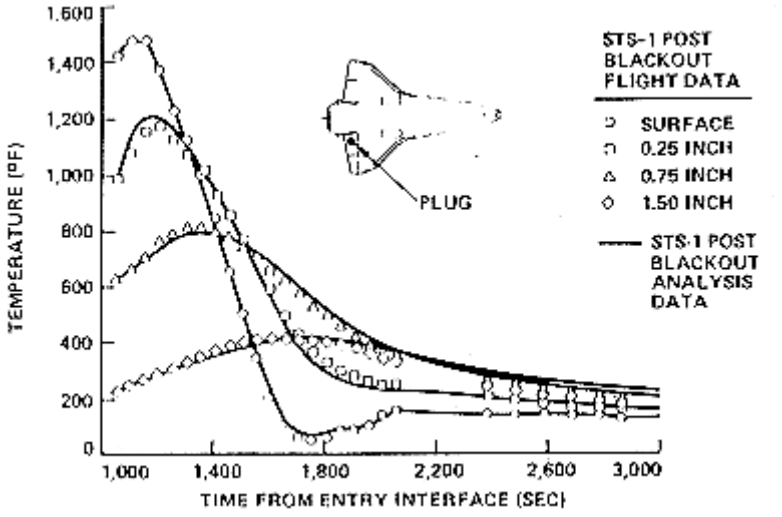

Note: non-si units are used in this figure

Figure 6-13: STS-1 flight data analysis comparison for lower inboard elevon location. From Dotts et al. (1983) [3].

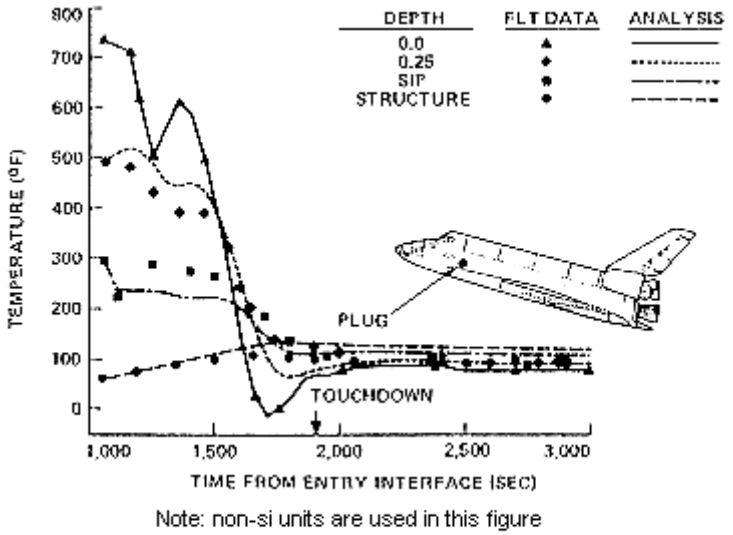

Figure 6-14: STS-1 flight data analysis comparison for lower mid-fuselage side location. From Dotts et al. (1983) [3].

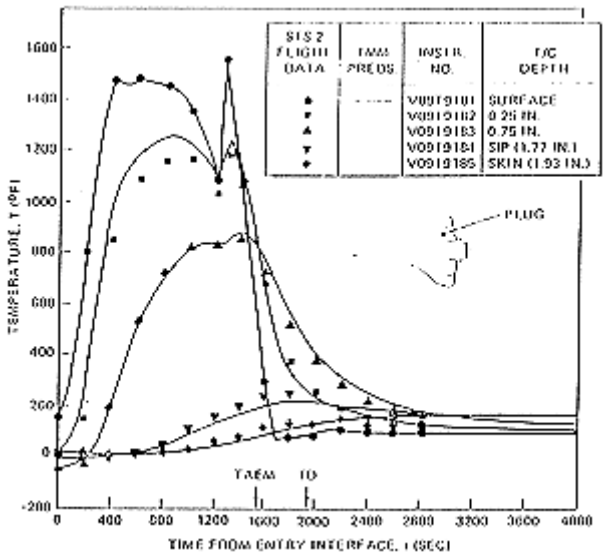

Figure 6-15: Comparison of STS-2 data with analytical predictions. From Normal et al. (1983) [11].

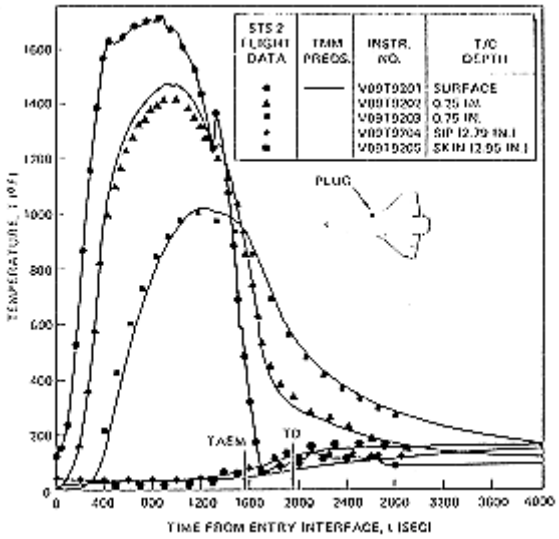

Figure 6-16: Comparison of STS-2 data with analytical predictions. From Normal et al. (1983) [11].

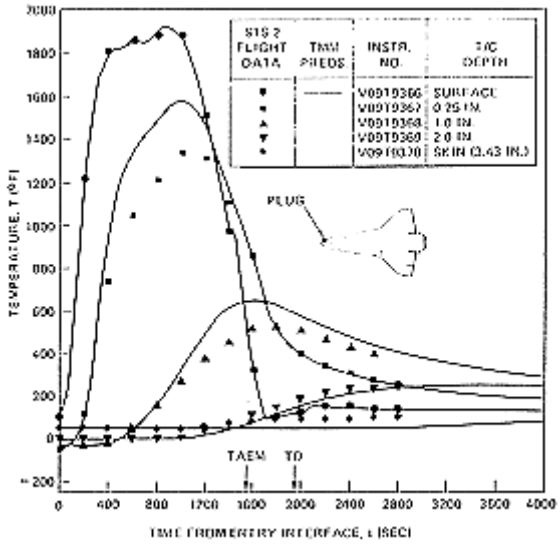

Figure 6-17: Comparison of STS-2 data with analytical predictions. From Normal et al. (1983) [11].

A plot of temperature vs. distance from the surface of the tile is shown in Figure 6-18.

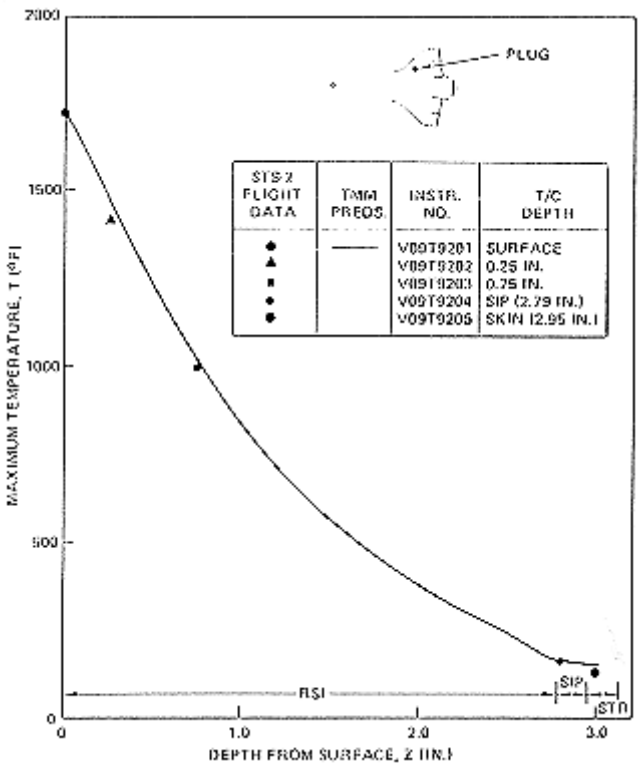

Note: non-si units are used in this figure

Figure 6-18: In-depth comparison of STS-2 data with analytical predictions for maximum temperatures. From Normal et al. (1983) [11].

6.4 Other developments

6.4.1 X-38

The X-38 was developed by the NASA-JSC as a prototype for a future Crew Rescue Vehicle (CRV). The size of the vehicle is limited in order to be launched by the Space Shuttle where it has to fit into the cargo bay. The X-38 shape is based on the X-24 lifting body flown at Dryden from 1969 to 1971. Wingless lifting bodies generate aerodynamic lift by the shape of their bodies. Three prototype X-38s of approximately 80% of the planned size of the CRV have been used in the atmospheric flight testing program. The orbital flight model corresponds to 100% CRV size and is being integrated at the Johnson Space Centre, Houston, Texas.

Due to its small size and lifting body shape and trajectory all surfaces will receive relatively high heat fluxes. Surface temperatures in the stagnation region are calculated to reach 1750°C, which is significantly higher than on the shuttle. Large areas of the central fuselage will be exposed to flow of hot gases around the vehicle. Temperatures of the forward fuselage upper surface are calculated to reach up to 1000°C and the application of a high temperature blanket thermal protection system (TPS) becomes mandatory. Consequently, the temperature level of the central and aft fuselage upper surface and of the base area will be significantly high. Unlike on the shuttle, where large areas of the surface are covered by flexible reusable surface insulation (FRSI), locations with surface temperatures below 400°C will be scarce on the X-38.

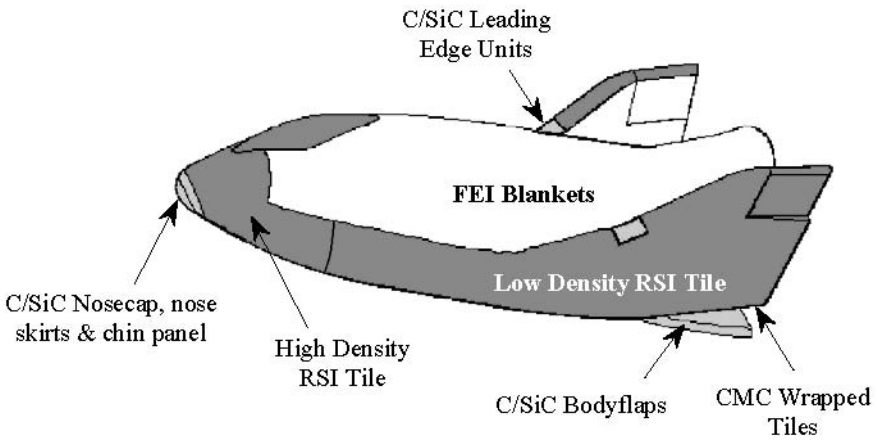

Figure 6-19: X-39 TPS Configuration

The initial TPS material selections for the various regions of the X-38 vehicle (Figure 6-19) were based upon early aerothermodynamic heating calculations. These calculations predicted that the majority of the lower surface of the vehicle would experience heating less than 96 W/cm^2 (85 BTU/ft^2-sec) (Figure 6-20). Based upon this maximum heating rate, and heating & pressure distributions calculated using computational fluid dynamics (CFD), a combination of ceramic matrix composite (CMC) components and ceramic silica-based tiles were selected for use on the lower surface. This selection does not preclude reusability, and builds on the extensive flight experience that has been gained on the Space Shuttle Orbiters. As the X-38 aerodynamic shape is based upon the X-23/X-24A, the TPS outer mold line (TOML) was the starting point for the TPS and structural design. The general shape of the structural outer mold line (SOML) was chosen to facilitate rapid computer aided design (CAD) of the SOML, as well as the manufacturing and assembling of the structure. For example, some portions of the lower structure surface are flat, and much of it has single curvature. Also, the lower surface is transitioned to the upper portion using simple conic surfaces. For the upper surface, the heating rates in this wake region are reduced to a level that allows the use of TPS blankets.

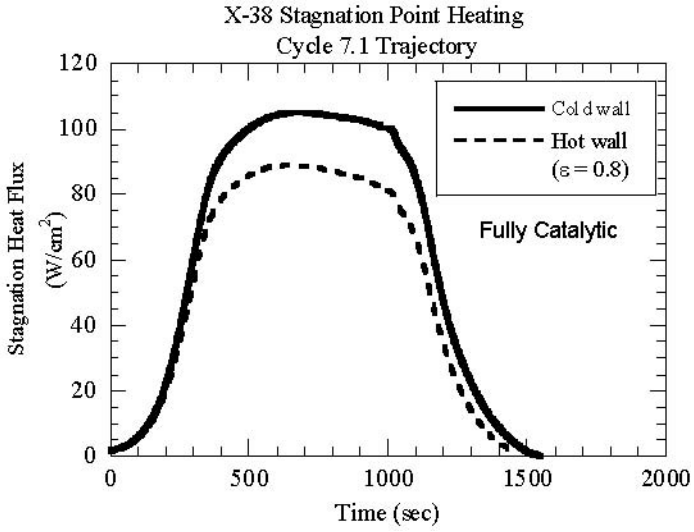

Figure 6-20: X-38 Reference Heating

6.4.1.1 Description of thermal protection subsystem

6.4.1.1.1 Carbon Silicone Carbide (C/SIC)

Nose Cap with CMC attachments

(TBD)

Nose Skirt with Metallic Attachments

Based on the experience with large CMC panel TPS a lightweight design concept on the front section of the X-38 was developed. Thermal analysis turned out that close behind the CMC nose cap the thermal load for the shuttle type tiles on the windward side reaches the critical temperature. Furthermore, the X-38 vehicle should be used to demonstrate the future technology on durable TPS for the CRV. Following this philosophy two large side panels were proposed for the actual X-38 configuration to replace the first row of tiles: The Nose Skirt Side Panels (see Figure 6-19). The gap between the two side panels is closed by a small C/SiC chin panel.

For the design of the 3 dimensional curved and large side panels including the stand-off fastener concept, considerable design and analysis effort had to be spent to find an appropriate TPS to the already defined cold structure. The thermal expansion of the CMC panel should be compensated by a system of flexible metallic stand-offs. An optimum in flexibility and stiffness to solve all requirements had to be found: strong and stiff enough to carry the thermo-mechanical loads, but flexible enough to realise a fastening concept which does not fail due to thermal expansion.

The manufactured qualification model of the nose skirt side panels, the metallic stand-offs and fasteners demonstrate the feasibility of this concept.

The fastening concept has been tested on development test level. Some thermal and mechanical tests on sub-structure level and the qualification tests have been performed with successful results .

The main objective of the X-38 program was to develop the technology for a prototype emergency Crew Return Vehicle (CRV), the lifeboat for the International Space Station (ISS). However, the project provides a good possibility to demonstrate already developed technology for future spacecraft.

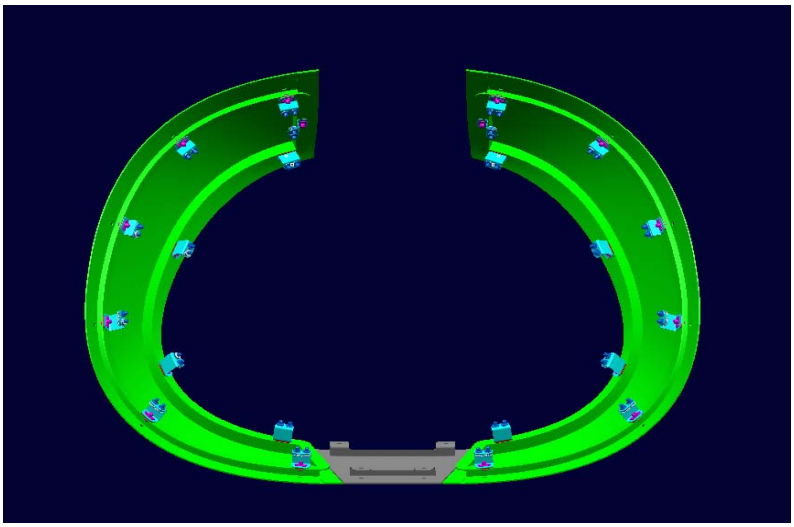

Figure 6-21: CMC Side Panels together with lower CMC Chin Panel

Since the heat loads in the area directly downstream the Nose Cap are still very high, the tile system was considered as not capable to withstand the temperatures. Therefore the first row of tiles has been replaced by a C/SiC panel TPS consisting of two large side panels and one small chin panel (see Figure 6-21).

Design of X-38 Nose Skirt Side Panels

The three dimensional curved side panels are along the edges continuously reinforced by a stringer. The wall thickness is still very small (t=3,5 mm) and not oversized to allow the flexible attachment system of the design concept: 11 flexible metallic stand-off fixations, connected to the C/SiC panel by PM 1000 fasteners.

Analysis Optimisation of Flexible Stand-offs and C/SiC Panel

The stand-offs have to:

— carry the pressure-, deformation- and gravitational loads

— reduce deformations

— be flexible enough to keep high margins in panel/ ceramic parts.

Additionally the stand-offs are loaded in torsion and shear which gives the constraint to optimise the width of stand-offs. The schematic view of the cross-section shows in Figure 6-22 that only little space between the CMC panel and the cold structure is left.

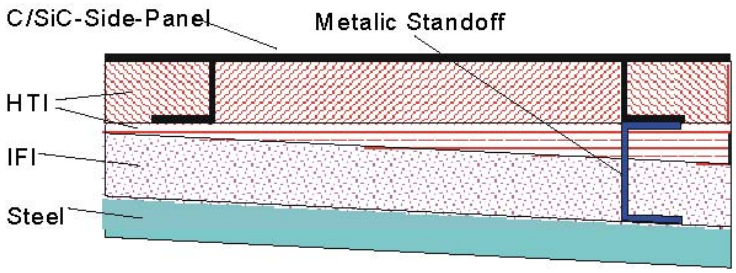

Figure 6-22: Stand-off Position and Global Design

The task is to reduce the stresses in the stand-offs while keeping stresses in ceramic parts and deformations at edges of the panel low. Optimisation by many FEM-calculations with varying number, positions and thicknesses of stand-offs led to a static over-determined design (shown in Figure 6-23).

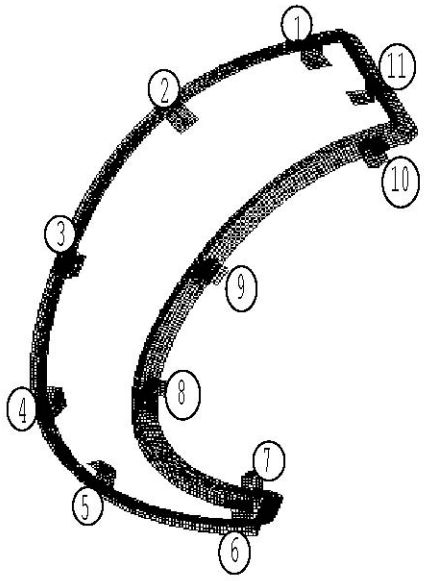

Figure 6-23: Stand-off Positions and Global Design

Structural analysis

The mesh of the nose skirt side panel was stepwise refined aiming at:

- evaluation of load introduction influences
- generation and evaluation of stresses in detailed section models
- simple variation of positions of stand-offs for optimisation
- calculation of buckling loads

The panel is subjected to very different kinds of loads:

- dynamical loads during ascent (cold)
- pressure loads during ascent induced by delayed compensation of atmospheric pressure (venting, cold)
- thermal loads caused by temperature and temperature gradients through the panel during descent overlaid by
- dynamical pressure loads during descent (hot)

The pressure loads during descent (shown in Figure 6-24) were calculated by aerodynamic formulae.

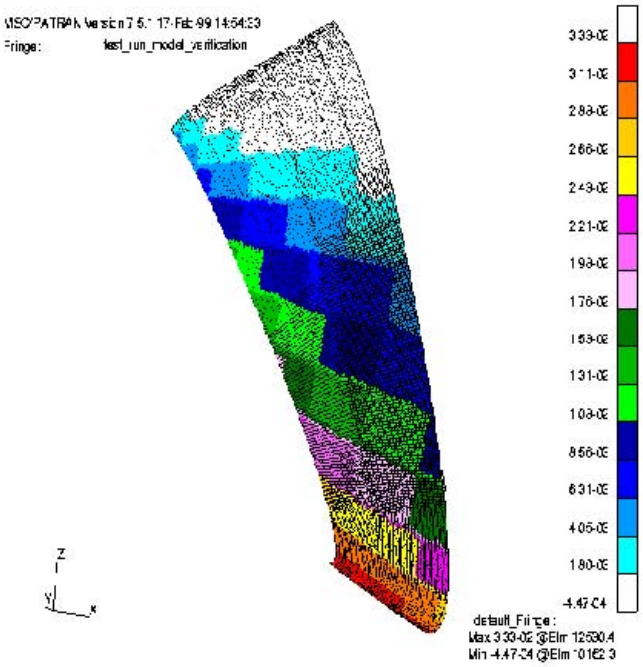

Figure 6-24: Max. Pressure Load

The thermal loads (shown in Figure 6-25) onto the structural model during descent were taken from the output of thermal analysis. The temperatures of the thermal mesh are applied to the grid points of the refined structural mesh by interpolation.

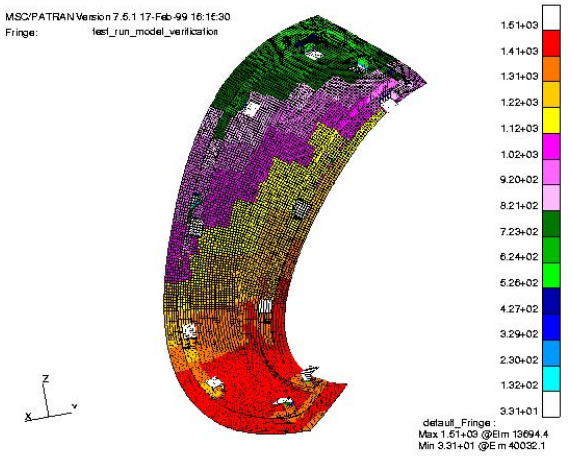

Figure 6-25: Max. Thermal Load at Panel Surface

Insulation Concept of the Nose Skirt Assembly

The C/SiC panels form the aerodynamic shape of the vehicle and provide protection to the exterior. The insulation is provided by a blanket insulation closing the gap between the panels and the substructure. An Internal Flexible Insulation (IFI), capable for re-use temperatures up to 1200°C, covers the metallic substructure. The IFI is protected on the hot side by a High Temperature Insulation (HTI) for temperatures up to 1650°C. Cut-outs are provided within the insulation blankets for the metallic fasteners of the C/SiC-panels and for the instrumentation. The insulation core is fabricated of

ceramic micro fiber felts. They are enclosed and sewn into ceramic fabrics. During the sewing process the fiber felts are compressed which leads to quasi elastic blankets. Figure 6-26 shows the Nose Skirt Assembly with the insulation.

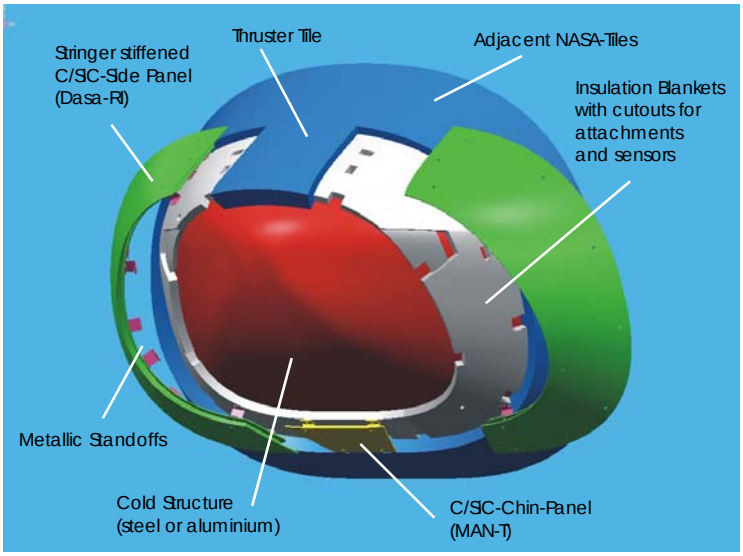

Figure 6-26: Nose Skirt Assembly with Insulation Blankets

Thermal Analysis

A three dimensional thermal mathematical model was developed containing one complete side with the stiffening stringers, the two different insulation materials IFI and HTI, the metallic substructure and the attachments for the fixation of the panel to the substructure.

Figure 6-27 shows the max. and min. heat flux timelines applied to the NSK.

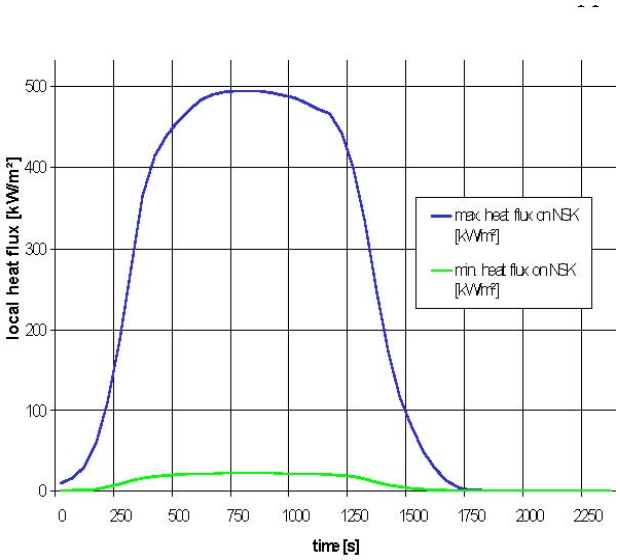

Figure 6-27: Max. and min. Heat flux time lines applied on the NSK

No convective cooling is considered during the gliding phase and postlanding. Radiation to space from the panel skin to the environment has been calculated assuming a constant radiation sink temperature of 4°C. A measurement based temperature dependant emissivity has been used for the panel coating in the range of 0.78 to 0.83. The steel substructure has been considered as heat barrier.

The thermal conductivity in the porous fiber insulation is calculated by approximation functions based on thermal conductivity measurements. These approximations describe the following heat transfer modes:

— the conductance through the fibers and through the fiber contact points

— the radiative heat transfer between the fibers as function of temperature

— the gas conductance within the pores between the fibers as function of temperature and air pressure

The different heat transfer mechanisms within the thermal model are depicted in Figure 6-28.

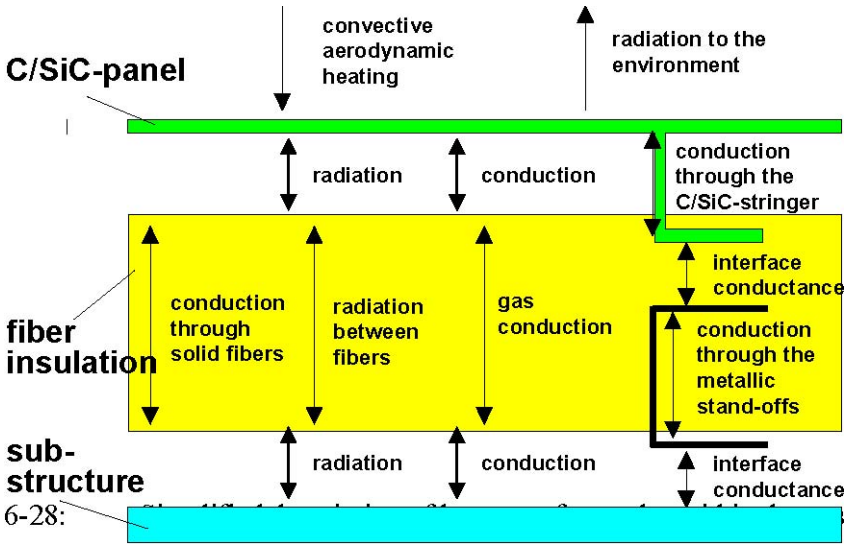

Figure 6-28: Simplified description of heat transfer modes within the nose skirt assembly.

Results of Thermal Analysis

The maximum occurring temperatures at thermo-mechanically critical locations within the NSK are listed in the following table.

	Maximum temperature during mission	Time of maximum temperature
C/SiC-panel within highest loaded area	1520°C	800s
C/SiC-panel within lowest loaded area	540°C	800s
Stringer flange in undisturbed area	1340°C	1200s
Metallic stand-offs	1110°C	1300s
I/F between HTI to IFI	810°C	1250s
Metallic substructure	80°C	4500s

Critical Load Cases

Critical load cases were identified for the stress analysis. Those cases result from the max. temperatures and temperature gradients over the panels, their stiffening stringers and over the stand-offs as well as the max. pressure loads and pressure gradients with time on the panels.

Temperature Distribution over the Side Panels

Figure 6-29 shows the temperature distribution over a side skirt panel at t=1100s. The figure shows the upside attachment plates of the metallic stand-offs. Very high local temperature gradients over the panels occur. The figure also shows the inhomogeneous temperature distribution at the stringer flanges caused by the cooling effect of the stand-offs which act as a heat bridge to the cold substructure.

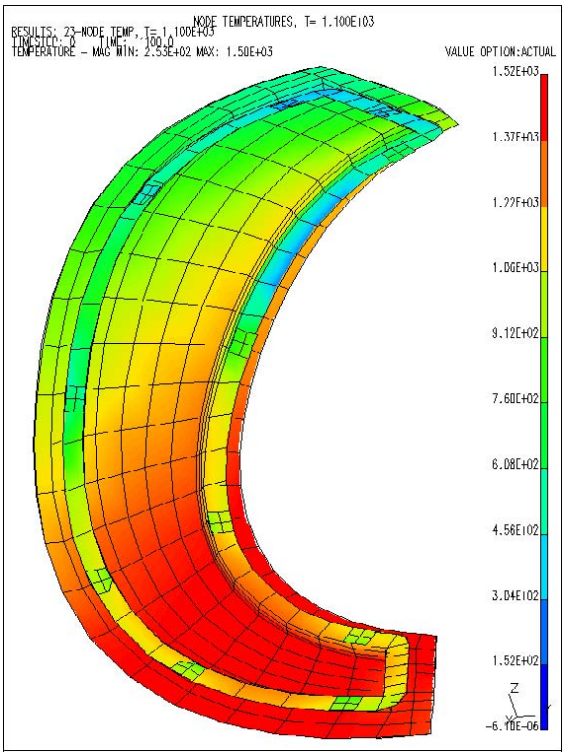

Figure 6-29: Temperature distribution over a NSK side panel at t = 1100s.

6.4.1.1.2 Flexible external insulation (FEI)

Introduction

This clause presents the design of the flexible blanket TPS for X-38. The design process had to consider aerothermal loads and constraints of the structure and parachute subsystems. NASA provided the configuration of the FEI assembly and the requirements design of the FEI blankets. The design concept and lay-out of the FEI-assembly was one of the European contribution to X-38. The FEI design is driven by the aeroshell panel design that distinguishes acreage panels, carrier panels and close-out areas, with dedicated blankets for each. Close out areas cover the locations of the parafoil system and create an uneven surface requiring vaulted blankets. The total of these requirements leads to an assembly of a large number of blankets, many of which have a complex shape. Proceeding from NASA furnished model files, the design to manufacturing of the FEI-blankets was established. In addition a test program has been performed for delta qualification of the FEI for X-38 application.

The FEI assembly is one of the European contributions to the X-38. This contribution comprises the conceptual design of the FEI, thermal analysis, manufacturing design, manufacturing of blankets and integration support. FEI covers most of the upper surface of the vehicle and the base. Three material systems have been chosen: the FEI-450, FEI-650 and FEI-1000, capable of limit temperatures of 450°C, 650°C and 1000°C, respectively.

The TPS blankets were initially sized with only two discrete thicknesses. While this results in overdesign for many areas, it also greatly simplifies the design, manufacturing and installation of the

TPS blankets, as well as the integration of the parafoil system. Without this simplification, transitioning from one blanket thickness to another requires ramping the substrate, usually with silicone adhesive and wedge-shaped felt insulation. This adds weight and increases installation time and complexity. Having limited blanket thicknesses will also reduce setup time for blanket manufacturing. Based on the preliminary heating environment distribution, it was determined that a

blanket thickness of 41 mm (1.6 in) would be used for that portion of the upper surface which is forward of the aft bulkhead, while a thickness of 25 mm (1.0 in) would be used aft of the aft bulkhead. The aft bulkhead was designed with a step in its upper flange to accommodate this blanket thickness transition. The blanket thickness change to 25 mm in the aft was in part due to a requirement to maximize volume in the fin to provide for the mechanism and actuator that will be used to fold the fin during launch.

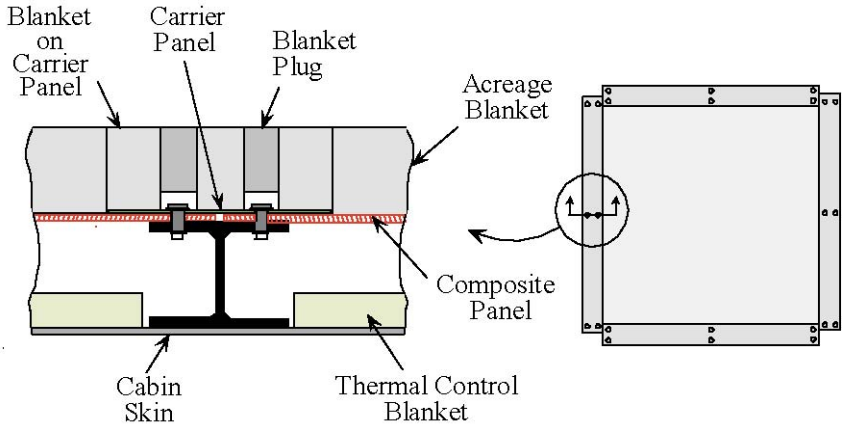

Figure 6-30: Carrier Panel TPS Design

The basic structure of the X-38 is constructed of machined aluminum frames and longerons. These frames and longerons are bolted together to form an airframe to which the aeroshell panels and various other vehicle system components are attached. The outer aeroshell of the V-201 is comprised of a combination of composite laminate panels, approximately 1.5 m by 1.5 m (5 ft by 5 ft) wide, and aluminum waffle panels. The TPS is directly bonded to these aeroshell panels. Subsystem installation and maintenance requirements demand that the panels be easily removable. This requirement necessitated extensive use of carrier panels to allow access to the numerous composite panel fasteners, as shown in Figure 6-30. These carrier panels are made of 2.5 mm (0.1 inch) thick composite laminate, requiring the carrier panel blankets to be reduced in thickness by this amount. To remove an aeroshell panel, the surrounding carrier panels are first detached by removing the limited number of carrier panel fasteners. This provides access to the numerous fasteners that attach the aeroshell panel, which are placed at a pitch of approximately 57 mm (2.25 inches), and the aeroshell panel can subsequently be removed.

With this requirement in place, much of the FEI blanket layout was predetermined. In simple acreage areas with no penetrations, the FEI blanket was designed to cover the entire panel up to the boundaries created by the surrounding carrier panels. In some cases the acreage panel blanket had to be split in two due to manufacturing restrictions on the maximum allowable blanket width. This can be seen in Figure 6-31, which shows the final FEI blanket layout. Also shown in the figure is the aeroshell panel layout, to illustrate its influence on the TPS design.

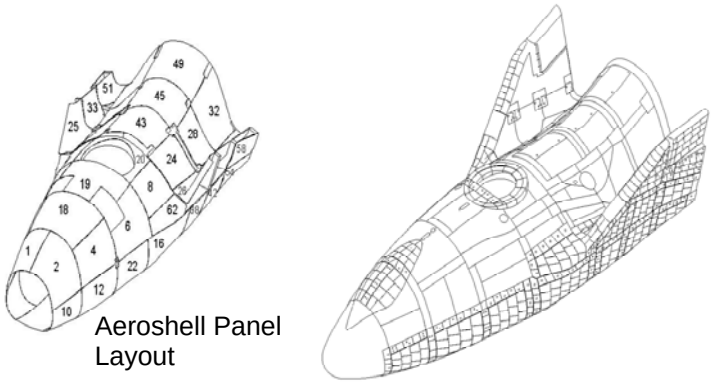

Figure 6-31: X-38 Aeroshell Panel and Blanket Distribution

Close-out Blanket Design

The X-38 will utilize a parafoil system (Figure 6-32) in conjunction with a skid landing gear system for landing. The parafoil lines will be made of several stacked layers of Kevlar® webbing straps, approximately 44 mm (1.75 inches) wide, and will require routing along the exterior of the aeroshell composite panels due to the relative locations of the parafoil container, parafoil fittings, drogue system and backup system (Figure 6-33). The blanket design is required to accommodate and thermally protect these parafoil lines. This requirement had a major impact on the design of the FEI blankets. The acreage blankets were designed leaving paths for the parafoil line routing. In order to determine the routing paths, lines were individually placed on the actual X-38 aeroshell to determine the twists and turns they would be required to make. Measurements were then taken and this information was modeled in a CAD system. The closeout blankets were designed using these CAD models, with seams determined to allow proper deployment of the lines for all possible scenarios. In order to ramp up to the parafoil lines, a foam material was selected that will be shaped and bonded to the aeroshell adjacent to the lines, providing a semi-continuous bonding surface for the closeout blankets. However, the blankets will be required to span the distance over the parafoil lines without being bonded for this distance.

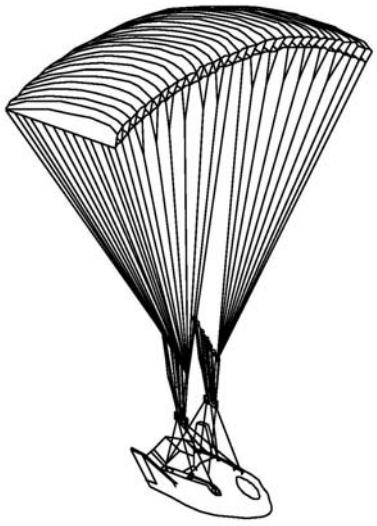

Figure 6-32: X-38 Parafoil System

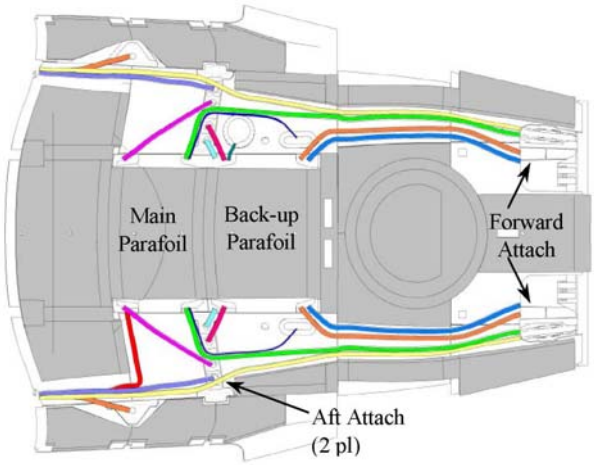

Figure 6-33: Parafoil Line Routing and Acreage Blankets

FEI-TPS Characteristics

Flexible blanket TPS, like the FEI, is the most lightweight TPS available up to date. The FEI blanket is a simple easy to apply and surprisingly sturdy component. It is adaptable to complex substructures and changing requirements without difficulties. In comparison to other TPS, the effort for manufacturing, integration and maintenance is low. Deteriorated blankets and damages are easily detected and the blanket is replaced with little effort. However, the application of FEI is limited to the leeward side. Due to its textile structure, flexible blanket TPS exhibits a porous and wavy surface of poor aerodynamic quality. This prohibits the application of FEI on the windward side of the vehicle.

The available range of FEI products is defined below by limit and ultimate temperatures (T_{lim}, T_{ult}) and construction. Increasing temperature capability goes hand-in-hand with increasing mass and cost of the blanket. The application temperature T_{lim} corresponds to 100 reentry cycles and moderate acoustic loads (OASPL=155dB):

FEI-300 - T_{lim}=300°C, T_{ult}=400°C - Assembly of gradient blankets made of two layers of aramide polymeric fiber needled felt reinforced by sewing with thread according to FEI technology.

FEI-450 - T_{lim}=450°C, T_{ult}=550°C - Assembly of functional gradient blankets made by stacking of two layers of aramide felts of adequate properties and poly-benzimidazole-fiber-felt (PBI), reinforced by sewing with silica thread. A typical Blanket is shown in Figure 6-34.

FEI-650 - T_{lim}=650°C, T_{ult}=850°C - Assembly of blankets made of silica felt, enclosed in ceramic fabrics and reinforced by sewing with ceramic thread. The principle design is depicted in Figure 6-35.

FEI-1000 - T_{lim}=1000°C, T_{ult}=1200°C - Assembly of blankets made of ceramic fiber felt, enclosed in ceramic fabrics corresponding to Figure 8 and reinforced by sewing with ceramic thread.

FEI-1100 - T_{lim}=1100°C, T_{ult}=1400°C - Assembly of blankets made of ceramic fiber felt, enclosed in ceramic fabrics and reinforced by sewing with ceramic thread. Enhanced temperature durability is achieved by using higher alumina content fibers.

IFI-1100 is used as internal flexible insulation (IFI) blanket for the C/SiC-Panel-TPS. - T_{lim}=1100°C, T_{ult}=1400°C - Design is similar to FEI-1100.

The blanket normally will be equipped with an organic water proofing and a silica based surface coating. Two coatings have been qualified so far, the white high reflectance coating ERN-MC-2S and the gray high emittance coating ERN-MC-6S

Figure 6-34: FEI-450 Blanket equipped with Gray FEI-1000High Emittance Coating

Figure 6-35: Typical look of FEI-650 and Blanket with Gray High Emittance

FEI-TPS Design Approach

At the beginning, a geometry model of the vehicle has been generated for the design analysis of the FEI-TPS. The mesh has been chosen compliant to the format of the aerothermal input data. Heating calculations have yielded a map of surface temperatures.

The design process runs according to three distinguished tasks:

— The calculation of surface temperatures based on aerothermal loads and the selection of blanket type to be applied in dedicated areas

— The analysis of critical locations in order to verify that the specific location is sufficiently insulated

— The manufacturing design of blankets based on the requirements design established by NASA and received in form of model files in the STEP exchange format.

Selection of Blanket Type

A geometrical model of the X-38 has been established of triangular surface elements according to the aerothermal loads. Due to the good insulation of the blankets, the thermal balance of the FEI surface is almost entirely depending on the equilibrium of the aero-convective heat flux to the surface and the heat radiated to the environment. The radiated heat depends on the emittance of the external surface. For the X-38 the gray coating ERN-MC-6S was chosen to cover the external face of the blanket. Aerothermal loads are provided for a constant emittance of $\varepsilon = 0.80$ and, were corrected with respect to the real emittance which is $\varepsilon = 0.85$ at room temperature and slightly decreases with increasing temperature. The calculation of surface temperatures takes respect to the radiation exchange between the surfaces of the vehicle. A 'THERMICA'-model of the X-38 was generated and used to determine the radiation exchange factors. The temperature calculations are performed by an 'ESATAN'-model taking respect to the radiation heat exchange, attributing local heat flux timelines and temperature dependant surface emittance to each of the surface nodes. Temperatures are obtained by steady state runs at defined time steps. Maximum temperatures are identified and processed into a map of maximum surface temperatures. Calculations with and without radiative heat exchange showed that temperatures significantly increase in the 'valley' between the winglets and the aft fuselage (see Figure 6-31, panels 25, 33, 51 and 26, 34, 52), due to the obstructed view to the environment and radiation from mainly the hot wing leading edge.

The FEI blanket types are allocated to the X-38 lee-side surface according the limit temperatures of the blankets. Therefore, the map of surface temperatures is compared to the FEI blanket lay-out (Figure 6-31). Blanket types are extended to the boundaries of the acreages such that the temperature of the selected blanket will never exceed the limit. Figure 6-36 shows the arrangement of FEI blanket types to the upper surface and the base of the X-38.

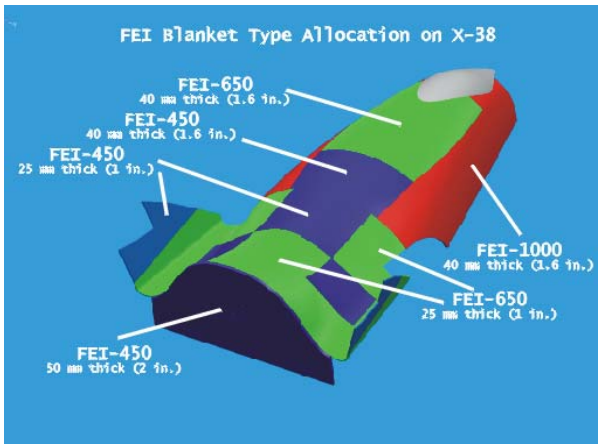

Figure 6-36: Allocation of Blanket Types to the X-38 Lee-Side Surface

Verification of Insulation

The blanket thickness at the different locations was defined by NASA as a consequence of TOML and SOML design, as explained above. Local analyses has been performed in worst case locations with ESATAN one-dimensional local models. In a first step it was shown, that in all cases the blanket thickness provides a comfortable margin. Therefore, in a second step it was agreed with NASA and ESA to reduce the density of the blankets, in order to save mass. The density of FEI-1000 and FEI-650 blankets core was reduced from originally 120kg/m^3 to 90kg/m^3. The density of the FEI-450 core was reduced from 120kg/m^3 to 110kg/m^3. In the third step it was demonstrated that in all cases, the insulation will be adequate.

CAD Methodology

The structure and TPS for the X-38 was designed using a CAD system. This includes the detailed design of approximately 1250 ceramic tiles and 136 FEI blankets, all referencing back to the original TPS outer mold line CAD surface model.

The actual manufacturing design concerns

- Complementation of design files by interfaces, and 'repair' of geometry, if necessary
- Transformation into the geometry to be actually manufactured
- Provision of CAM files for drawing and cutting of templates and milling of mock-ups
- Provision of CAM files for sewing of blankets.

Paper drawings are created from the draw mode of the CAD models solely for documentation and for inspection of the hardware and documentation of the as-built status.

Qualification for X-38

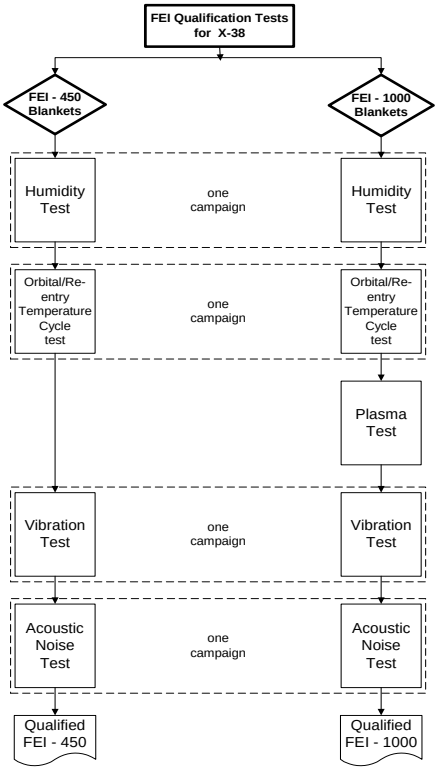

Figure 6-37: Qualification Test Sequence for X-38

FEI-1000	FEI-450
Ground Environment: • Humidity Test, hours	Ground Environment: • Humidity Test, hours
On-Orbit: • 12 cycles at 120°C < T < 150°C	On-Orbit: • 12 cycles at 120°C < T < 150°C
Re-Entry (Plasma Test): • 3 nominal cycles at 50°C < T < 1000°C with 20 min at 1000°C-lev • 1 ultimate cycle at 50°C < T < 1200°C with 20 min at 1200°C-lev	Re-Entry (IR-radiati facility): • 3 nominal cycles at 50°C < T < 450°C wi 15 min at 450°C-leve • 1 ultimate cycle at 50°C < T < 550°C wi 9 min at 550°C-level
Ascent: • Vibration • Acoustic Noise at 1 dB for 1.5 min.	Ascent: • Vibration • Acoustic Noise at 1 dB for 1.5 min.

Figure 6-38: Parameters and Results of the Qualification Tests

The qualification of the FEI-TPS for X-38 has considered three load cycles and a scatter factor of four with respect to a future CRV application. Additional verification has been achieved by characterization tests concerning thermal and mechanical properties. Acoustic noise tests have been used as the major tool for screening and mechanical characterization. Blankets with the improved coating have been exposed to extremely high dynamic loads to prove the structural integrity of the blanket-coating system. Absorptance, emittance and plasma compatibility concerning erosion and catalycity have been investigated for the new coating.

Figure 6-37: Qualification Test Sequence for X-38

Figure 6-38: Parameters and Results of the Qualification Tests

Figure 6-37 depicts the test sequence that has been followed for the delta qualification to X-38 requirements. The test sequence reflects the most severe environment concerning ascent in the shuttle cargo bay, orbital flight and reentry. The test parameters and results are summarized in Figure 6-38. The FEI-650 has not been tested here. Since the load carrying system is the same as on the FEI-1000, it is qualified by similarity to the FEI-1000 and by similarity to tests performed in the course of former programs. The structural verification to sinusoidal/ random vibration and acoustic noise testing is performed at the end of the sequence. Applying launch loads after all the environmental loads have been collected surely imposes a worst case. Additionally, at the end of the test sequence the samples have been exposed to increased acoustic levels to provide data about material strength and the margin to failure.

Manufacturing and Integration

The total requirement for V-201 calls for 136 blankets of the three types FEI-1000, FEI-650 and FEI-450. In addition, 207 plugs of five types are needed to close the access holes to the fasteners of the carrier panels.

Acreage panels normally are covered by large blankets of two-dimensional geometry. The existing equipment allows to manufacture blankets up to a size of 2.5 by 2.5 meters. Due to the strong geometrical requirements for X-38 blankets maximum dimensions have been limited to 1.2 meters by 1.8 meters. Figure 6-41 shows the sewing head of the computer controlled sewing machine in operation.

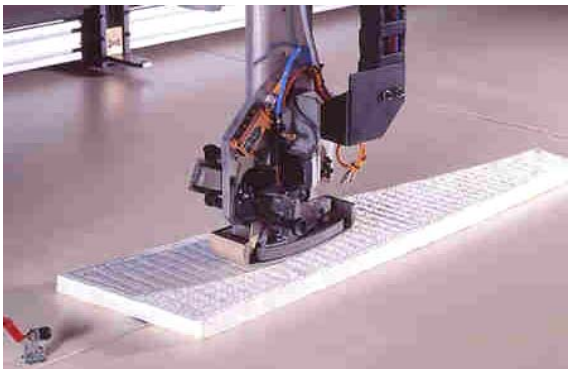

Figure 6-39: Computer controlled sewing of FEI blankets

The blankets of the 'valley' between winglet and aft fuselage are of complicated three-dimensional shape and require highest effort and precision to manufacturing. Carrier panel blankets generally are narrow strips and carry two to eight holes. Close out blankets are generally small but some of them are of complex shape due to an overlay of two three-dimensional geometries. Figure 6-40 shows an example of the FEI-1000 acreage blankets for the forward fuselage.

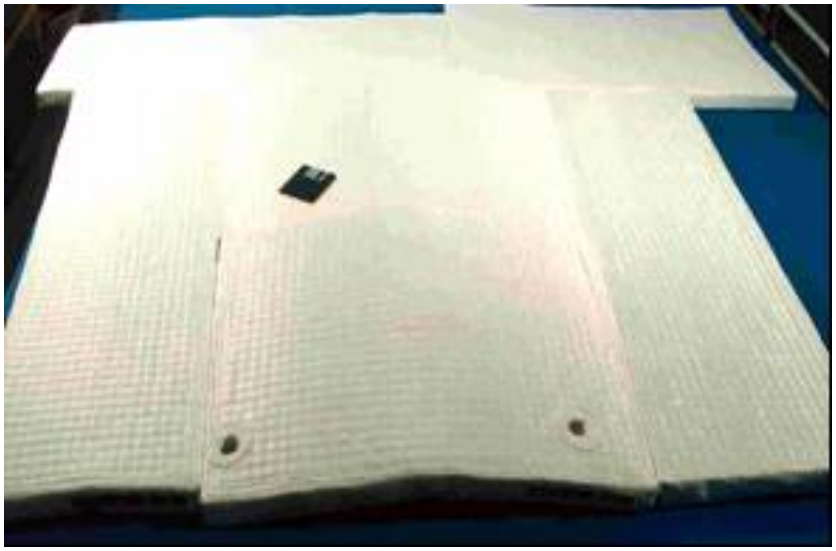

Figure 6-40: FEI-1000 blankets of the Forward Fuselage

Figure 6-41: FEI Blankets Integrated on the X-38 V-201

The integration of the FEI blankets was performed at the JSC. The blankets are first installed on the structural panels by adhesive bonding and then the panels are mounted to the vehicle. This work is performed by NASA experts. The blankets delivered have already been integrated, as can be seen from Figure 6-41. When integration of blankets will be completed, it is planned that ASTRIUM ST experts will apply the gray high emittance coating by the unique spray process developed for in-situ coating of large surfaces.

Bibliography

[1] Anderson, J.D., "Hypersonic and High Temperature Gas Dynamics", McGraw-Hill, 1989.

[2] Antonenko, J., Ebeling, N., Schwarz, B., Menn, F., "Lightweight Fiber Insulations Performance and Application", ESA SP-324, Dec. 1991.

[3] Curry, D.M., Cunningham, J.A., Frahm, J.R., "Space Shuttle Orbiter Leading Edge Thermal Performance", Progress in Aeronautics and Astronautics, Vol. 85, pp. 206-233, 1983.

[4] Delahais, Nerault, "The Hermes System: Programme Status and Technology Aspects", Acta Astronautica, Vol. 25, pp. 11-22, 1991.

[5] Dotts, R.L., Battley, H.H., Hughes, J.T., Neuenschwander, W.E., "Shuttle Orbiter Reusable Surface Insulation Thermal Performance", Progress in Aeronautics and Astronautics, Vol. 85, pp. 183-205, 1983.

[6] East, R.A., "Atmospheric Re-Entry", in "Spacecraft Systems Engineering", clause 12. Peter Fortescue & John Stark (Eds.), Wiley, 1991.

[7] Goodrich, Derry, Maraia, "Effects of Aerodynamic Heating and TPS. Thermal Performance Uncertainties on the Shuttle Orbiter", Progress in Aeronautics and Astronautics, Vol. 69, pp. 247-268, 1980.

[8] Green, M.J., Davy, W.C., "Galileo Probe Forebody Thermal Protection", Progress in Aeronautics and Astronautics", Vol. 82, pp. 328-353, 1982.

[9] Hurwicz, H., Rogan, J.E., "High-Temperature Thermal Protection Systems", Handbook of Heat Transfer, Clause 59, W.M. Rohsenow and J.P. Hartnett (Eds.), McGraw-Hill, 1973.

[10] Hurwicz, H., Rogan, J.E., "Ablation", Handbook of Heat Transfer, Clause 56, W.M. Rohsenow and J.P. Hartnett (Eds.), McGraw-Hill, 1973.

[11] Norman, I., Rochelle, W.C., Kimbrough, B.S., Ritrivi, C.A., Ting, P.C., Dotts, R.L., "Comparison of Orbiter STS-2 Development Flight Instrumentation Data with Thermal Math Model Predictions", Progress in Aeronautics and Astronautics, Vol. 85, pp. 234-254, 1983.

[12] Vialaneix, J., Nerling, E., Verneuil, J., "Structures Chaudes et Protections Thermiques de L'Avion Spatial Europeen Hermes", Proceedings of the 4th Symposium on Space Environmental and Control Systems, ESA SP-324, Dec. 1991.

[13] Ulrich Trabandt, Thomas Schmid, Hans-Georg Wulz, Heiko Ritter, Heiko Reinhober: "CMC Large Panel TPS Applied on X-38 Nose Skirt", SAE Technical Paper 2000-01-2234

[14] NASA Facts - X-38, http://www.dfrc.nasa.gov/PAO/PAIS/HTML/FS-038-DFRC.html

[15] Campbell CH, Caram JM, Li CP and Madden CB; Aerothermodynamic Environment Definition for an X-23/X-24A Derived Assured Crew Return Vehicle; AIAA Paper 96-1862, June 1996.

[16] Rasky D. J.; Thermal Protection Systems for Future Reusable Launch Vehicles; 25th Int. Conf. Env. Syst., San Diego, Ca, 1995

[17] Jones F. E.; The Cost of Maintaining Thermal Protection System; Space Shuttle Development Conf., Moffett Field, CA, July 1999

[18] Behrens B. et al.; Flexible External Insulation on X-38 ; SAE-1999-01-2167